Molecular Therapy

Original Article

Reversion of metabolic dysfunction-associated steatohepatitis by skeletal muscle-directed FGF21 gene therapy

Veronica Jimenez,[1,2,3,11] Victor Sacristan,[1,2,3,11] Claudia Jambrina,[1,2,3] Maria Luisa Jaen,[1,2,3] Estefania Casana,[1,2,3] Sergio Muñoz,[1,2,3] Sara Marcó,[1,2] Maria Molas,[1,2,3] Miquel Garcia,[1,2,3] Ignasi Grass,[1,2,3] Xavier León,[1,2,3] Ivet Elias,[1,2,3] Albert Ribera,[1,2] Gemma Elias,[1,2] Victor Sanchez,[1,2] Laia Vilà,[1,2,3] Alba Casellas,[1,2,3] Tura Ferre,[1,2,3] Jordi Rodó,[1,2] Ana Carretero,[1,4] Marti Pumarola,[1,5] Marc Navarro,[1,4] Anna Andaluz,[5] Xavier Moll,[5] Sonia Añor,[5] Sylvie Franckhauser,[1,2,3] Mercedes Vergara,[6,7,8,9] Assumpta Caixàs,[6,7,10] and Fatima Bosch[1,2,3]

[1]Center of Animal Biotechnology and Gene Therapy (CBATEG), Universitat Autònoma de Barcelona, 08193 Bellaterra, Spain; [2]Department of Biochemistry and Molecular Biology, Universitat Autònoma de Barcelona, 08193 Bellaterra, Spain; [3]Centro de Investigación Biomédica en Red de Diabetes y Enfermedades Metabólicas Asociadas (CIBERDEM), 28029 Madrid, Spain; [4]Department of Animal Health and Anatomy, School of Veterinary Medicine, Universitat Autònoma de Barcelona, 08193 Bellaterra, Spain; [5]Department of Animal Medicine and Surgery, School of Veterinary Medicine, Universitat Autònoma Barcelona, 08193 Bellaterra, Spain; [6]Institut d'Investigació i Innovació Parc Taulí (I3PT-CERCA), 08202 Sabadell, Spain; [7]Department of Medicine, Universitat Autònoma de Barcelona, Teaching Unit Parc Taulí, 08202 Sabadell, Spain; [8]Department of Hepatology, Digestive Service, Hospital Universitari Parc Taulí, 08202 Sabadell, Spain; [9]Centro de Investigación Biomédica en Red de Enfermedades Hepáticas y Digestivas (CIBEREHD), 28029 Madrid, Spain; [10]Department of Endocrinology and Nutrition, Hospital Universitari Parc Taulí, 08202 Sabadell, Spain

The highly prevalent metabolic dysfunction-associated steatohepatitis (MASH) is associated with liver steatosis, inflammation, and hepatocyte injury, which can lead to fibrosis and may progress to hepatocellular carcinoma and death. New treatment modalities such as gene therapy may be transformative for MASH patients. Here, we describe that one-time intramuscular administration of adeno-associated viral vectors of serotype 1 (AAV1) encoding native fibroblast growth factor 21 (FGF21), a key metabolic regulator, resulted in sustained increased circulating levels of the factor, which mediated long-term (>1 year) MASH and hepatic fibrosis reversion and halted development of liver tumors in obese male and female mouse models. AAV1-FGF21 treatment also counteracted obesity, adiposity, and insulin resistance, which are significant drivers of MASH. Scale-up to large animals successfully resulted in safe skeletal muscle biodistribution and biological activity in key metabolic tissues. Moreover, as a step toward the clinic, circulating FGF21 levels were characterized in obese, insulin-resistant and MASH patients. Overall, these results underscore the potential of the muscle-directed AAV1-FGF21 gene therapy to treat MASH and support its clinical translation.

INTRODUCTION

Metabolic dysfunction-associated steatotic liver disease (MASLD) is the most common chronic hepatic disorder worldwide, reaching epidemic proportions with a prevalence of 11%–37% in the adult population.[1,2] MASLD initiates as excessive accumulation of lipids in the liver that progresses toward severe metabolic dysfunction-associated steatohepatitis (MASH), characterized by ≥5% hepatic steatosis with inflammation, hepatocyte injury, and fibrosis.[2,3] At advanced stages, MASH is associated with severe liver disease, such as cirrhosis, hepatocellular carcinoma (HCC), and end-stage liver disease, and with increased mortality rate.[4] The global epidemics of obesity and type 2 diabetes (T2D) are important risk factors for MASH.[1,5,6] In the United States and European Union, about 40 million people are afflicted by MASH.[7]

Despite the increasing prevalence of MASH, until very recently no pharmacotherapies were available and it has been considered an unmet medical need. In March 2024, the FDA approved resmetirom (Rezdiffra), an oral thyroid hormone receptor β agonist, under the accelerated approval pathway, for adults with MASH with moderate to advanced fibrosis.[8,9] Nevertheless, in the phase 3 MAESTRO-NASH trial, just 25%–30% of patients treated with resmetirom showed improvement of the two primary endpoints at week 52.[10] Therefore, because of the heterogeneous nature of the disease and its high prevalence, additional safe, effective, and durable treatment modalities are needed for MASH.
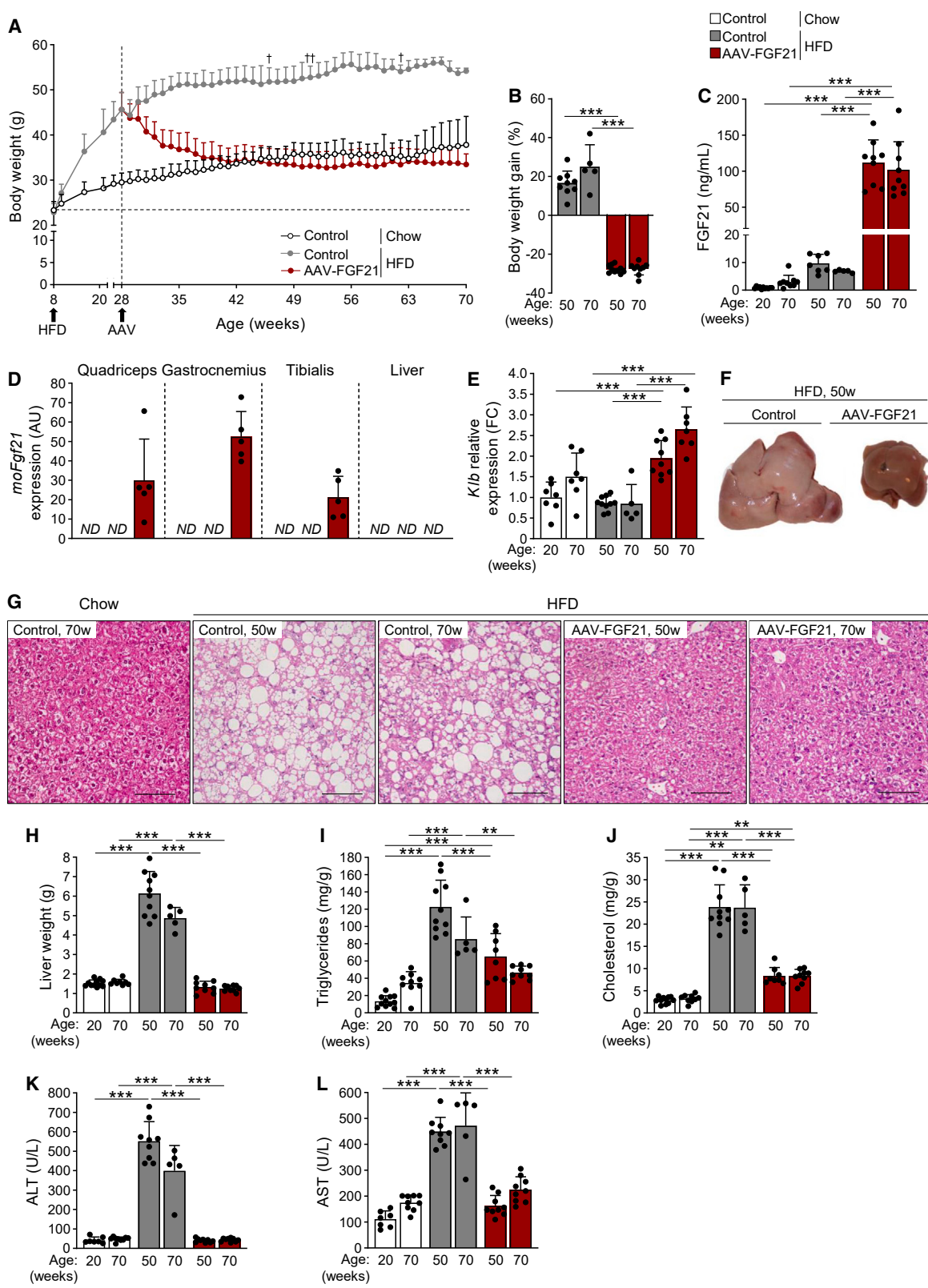
Gene therapy may deliver transformative benefits for MASH patients. Multiple adeno-associated viral (AAV) vector-based gene therapies

(legend on next page)

have been shown to provide definitive therapeutic benefit for monogenic diseases in the clinical setting.[11,12] AAV vectors, derived from non-pathogenic viruses, are predominantly non-integrative and able to mediate multi-year generation of therapeutic proteins after a single administration.[11–17] Such breakthroughs in genetic therapy for rare diseases have laid the groundwork for the development of AAV-based treatments for complex, polygenic, and highly prevalent metabolic diseases.

Fibroblast growth factor 21 (FGF21) may be a promising candidate gene to revert MASH since it regulates energy homeostasis and exerts anti-inflammatory and anti-fibrotic effects in multiple tissues, including the liver.[18–20] Moreover, liver or adipose tissue-directed AAV-FGF21 gene therapy enables a long-lasting increase in native FGF21 levels in circulation, resulting in sustained counteraction of obesity and insulin resistance in mice.[21] However, in the clinical setting, mild to severe renal, liver, and dorsal root ganglia toxicities, thrombotic microangiopathies, and heart and lung failure, leading in some cases to fatalities, have recently been documented following systemic intravenous administration of high doses of AAV vectors.[22–26] This is of particular importance in diseases such as MASLD and MASH, where there is significant pre-existing liver damage and increased risk for HCC.[27] In contrast, animal and human data show that genetic engineering of skeletal muscle by intramuscular (IM) administration of AAV vectors is safe, well tolerated, and leads to minimal systemic biodistribution.[13–17,28] Skeletal muscle has additional advantages as a target tissue for AAV-mediated gene transfer since it is easily accessible by noninvasive procedures and enables efficient and long-term sustained expression of therapeutic proteins because of the low replication rate of myofibers. To date, durability in large animals and humans has been documented for 8 and 10 years, respectively.[15,16] Moreover, gene delivery to muscle is not limited by the presence of preexisting neutralizing antibodies against AAV,[28–31] a key aspect given the relatively high prevalence of anti-AAV antibodies in the general population.[32]

Here, we demonstrate that IM AAV1-mediated genetic engineering of skeletal muscle with native FGF21 coding sequence resulted in durable increased circulating levels of the factor, which reverted established MASH, precluded progression from MASH to cirrhosis and HCC, counteracted obesity, and increased insulin sensitivity in obese mice. Scale-up to large animals also successfully resulted in secretion of active FGF21 and beneficial metabolic effects. As a step toward clinical translation, evaluation of FGF21 circulating levels in a cohort of 500 obese, T2D, and MASH patients revealed that most of this population would be eligible for the AAV-FGF21-mediated therapeutic approach. These results support non-clinical safety and efficacy and the advancement of AAV1-FGF21 as an investigational product for MASH patients.

RESULTS

High-fat diet feeding induces MASH in mice

To develop new effective therapies to revert MASH, mouse models closely resembling the human disease should develop liver steatosis, inflammation, and fibrosis prior to treatment administration.[33] Similarly to human patients, these mice should also present other key metabolic alterations, such as obesity, insulin resistance, and an altered adipokine profile.[33] To this end, 8-week-old wild-type male mice were fed a high-fat diet (HFD) for 12, 18, or 29 weeks to determine MASH development. After 12 weeks on HFD, mice became obese, showed enlarged liver, and severe hepatic steatosis with markedly increased hepatic triglycerides and cholesterol content (Figures S1A–S1E). Moreover, 12 weeks after initiation of HFD feeding, immunostaining of liver sections with the macrophage-specific marker MAC2 showed marked macrophage infiltration concordant with increased hepatic gene expression levels of the cell surface proteins CD68 antigen (Cd68; a marker of phagocytic macrophages) and adhesion G protein-coupled receptor E1 (Adgre1, also known as F4/80; a broad macrophage marker, likely Kupffer cells in the liver) (Figures S1E–S1G). Consistent with development of severe inflammation, marked hepatic fibrosis determined by Picrosirius red (PSR) staining and increased gene expression of the fibrosis markers collagen type 1α and type 3α (Col1a1 and Col3a1) were observed in the liver (Figures S1E, S1H, and S1I). Hepatic stellate cells (HSCs) are the primary fibrogenic cells involved in the progression of liver fibrosis in MASLD. During this process, HSCs become activated and acquire a myofibroblast-like phenotype characterized by expression of α-smooth muscle actin (a-Sma).[34,35] HFD-fed mice also showed markedly increased gene expression of a-Sma in the liver (Figure S1J). All these results demonstrated severe hepatic steatosis, inflammation, and fibrosis in HFD-fed mice, consistent with MASH development.

Reversal of hepatic steatosis in HFD-fed mice after IM administration of AAV-FGF21

The therapeutic potential of the AAV-based muscle-specific FGF21 gene therapy against MASH was evaluated in male mice that were fed an HFD for 20 weeks to induce MASH (Figure 1A).

Figure 1. AAV-mediated skeletal muscle gene transfer of FGF21 reverses hepatic steatosis
Eight-week-old male mice were fed an HFD. Twenty weeks later, mice were treated intramuscularly with AAV-FGF21 vectors and remained in HFD feeding for all experimental periods. Non-injected chow and HFD-fed mice were used as controls. (A) Body weight follow-up (n = 9–10/group). (B) Body weight gain in HFD-fed groups from weeks 28–70 of age (n = 5–10/group). (C) Serum FGF21 levels at different time points (n = 5–11/group). (D) Quantitative PCR analysis of murine optimized Fgf21 (moFgf21) expression in the three injected skeletal muscles and in the liver in 70-week-old male mice (n = 5–7/group). (E) Hepatic expression of Klb (n = 5–10/group). (F) Representative macroscopic images of the liver from control HFD-fed (left) and AAV-FGF21-treated (right) male mice at age 50 weeks. (G) Representative images of hematoxylin and eosin staining of liver sections at age 50 and 70 weeks. Scale bars, 100 μm. (H) Liver weight at different time points (n = 5–11/group). (I and J) Liver triglyceride (I) and cholesterol (J) content (n = 5–11/group). (K and L) Serum ALT (K) and aspartate aminotransferase (AST) levels (L) (n = 5–9/group). Data are presented as mean ± SD; **$p < 0.01$, ***$p < 0.001$ by one-way analysis of variance (ANOVA) with Bonferroni multiple comparison test. AU, arbitrary units; ND, non-detected; FC, fold change; w, weeks; †, death due to natural causes.

Twenty-eight-week-old obese animals received a dose of 3×10^{11} viral genomes (vg)/mouse (7×10^{12} vg/kg) of AAV vectors of serotype 1 encoding a murine optimized *Fgf21* coding sequence (*moFGF21*) under the control of the cytomegalovirus (CMV) promoter (AAV-FGF21) by IM administration distributed over the quadriceps, gastrocnemius, and tibialis muscles of both hindlimbs (Figure 1A). To assess therapeutic efficacy, two cohorts of AAV-FGF21-treated mice were maintained on HFD up to either age 50 or 70 weeks. As controls, non-vector-treated chow- and HFD-fed male mice were used. The mice treated with AAV-FGF21 showed a progressive reduction of body weight up to age 40 weeks, remaining indistinguishable from chow-fed mice thereafter, consistent with complete reversal of obesity (Figure 1A). From age 28–50 and 70 weeks, the body weight of HFD-fed non-treated mice increased by 18% and 30%, respectively, while that of animals treated with AAV-FGF21 decreased about 30% (Figure 1B).

Although HFD-fed untreated mice showed increased FGF21 serum levels compared with chow-fed mice (Figure 1C), this increase was not able to decrease their body weight gain (Figures 1A and 1B). Normalization of the obese phenotype resulted from about 10-fold increased circulating FGF21 levels achieved after treatment of HFD-fed mice with AAV-FGF21 (Figure 1C). The high circulating FGF21 resulted primarily from expression of *moFGF21* from the vector-transduced skeletal muscles (Figure 1D). As a result of the IM administration of AAV1 vectors, *moFGF21* expression was not detected in other tissues, such as the liver (Figure 1D), as previously observed for other transgenes.[16,17] In agreement with increased serum FGF21, gene expression of the FGF21 co-receptor β-klotho (*Klb*), which is essential for FGF21 signaling,[36] was markedly increased in the liver of AAV-FGF21-treated mice (Figure 1E).

Hepatomegaly was also normalized in HFD-fed AAV-FGF21-treated animals (Figures 1F–1H). Histological analysis of liver sections of HFD-fed mice revealed marked hepatic steatosis, which was fully reverted after treatment with AAV-FGF21 (Figure 1G), concurrent with reduction in the liver triglyceride and cholesterol content (Figures 1I and 1J). In agreement with reversal of hepatic steatosis, the activity levels of the hepatic injury markers alanine aminotransferase (ALT) and aspartate aminotransferase were normalized in AAV-FGF21-treated mice (Figures 1K and 1L). These results demonstrated that IM treatment with 3×10^{11} vg of AAV-FGF21 vectors mediated marked therapeutic benefit against fatty liver disease. Similarly, a marked reduction in body and liver weights and counteraction of hepatic steatosis were observed in HFD-fed female mice and also in ob/ob male and female mice treated with 3×10^{11} vg of AAV-FGF21 vectors (1×10^{13}, 7×10^{12}, and 7.4×10^{12} vg/kg, respectively) (Figures S2A–S2E and S3A–S3K).

Treatment with AAV-FGF21 reverts hepatic inflammation and fibrosis and halts development of liver tumors

Immunostaining of liver sections of untreated HFD-fed male mice with MAC2 showed marked macrophage infiltration, which was not detected in HFD-fed AAV-FGF21-treated animals (Figure 2A).

The lack of hepatic inflammation in these mice was parallel to normalization of gene expression levels of macrophage markers *F4/80* and *Cd68,* and of pro-inflammatory soluble cytokines, such as chemokine (C-C motif) ligands 2, 3, and 5 (*Ccl2, Ccl3,* and *Ccl5*) and tumor necrosis factor α (*Tnfa*) (Figures 2B–2G). Moreover, AAV-mediated FGF21 gene therapy reverted hepatic fibrosis. Collagen fibers were abundant in the liver of old HFD-fed mice because of the very advanced fatty liver disease (Figure 3A). Histomorphometric quantitative assessment of liver fibrosis using PSR staining indicated complete fibrosis reversal 22 weeks post treatment (Figure 3B). Gene expression levels of *Col1a1* and *Col3a1* were also increased in nontreated HFD-fed mice but normalized in AAV-FGF21-treated mice (Figures 3C and 3D). mRNA levels of *Col1a1* and *Col3a1* as well as of other fibrotic markers analyzed (*vide infra*) were decreased at age 70 weeks in HFD-fed male mice compared with those at age 50 weeks, likely due to significant progression of HCC and presence of liver tumors. HFD-fed female mice and ob/ob male and female mice treated IM with AAV-FGF21 vectors also showed counteraction of liver inflammation and fibrosis (Figures S2E–S2G and S3K–S3M).

In agreement with reversal of fibrosis, AAV-FGF21-treated male mice normalized the expression of genes involved in extracellular matrix deposition, including matrix metalloproteinases 12 and 13 (*Mmp12 and 13*) and tissue inhibitor of metalloproteinases 1 (*Timp1*) (Figures 3E–3G). Moreover, gene expression of the activated HSC marker *a-Sma* and of key cytokines involved in HSC activation, such as transforming growth factor β 1 (*Tgfb*) and platelet-derived growth factor α and β (*Pdgfa* and *Pdgfb*),[34] was similar to those of old healthy chow-fed mice (Figures 3H–3K). Together these findings indicated that the increase of muscle-derived FGF21 levels in circulation mediated MASH resolution.

Long-term feeding with HFD has also been associated with late-stage progression of MASH and increased incidence of liver tumors in C57BL/6J mice.[37] While half (5/10) and all (5/5) of the control HFD-fed mice developed liver tumors by age 50 and 70 weeks, respectively (Figure S4), none of the animals treated with AAV-FGF21 vectors developed tumors either at age 50 (0/9) or 70 (0/9) weeks. None of the chow-fed mice developed tumors during the follow-up period. Consistent with these results, HFD feeding induced a progressive expression of HCC markers, such as α-fetoprotein (*Afp*), lymphocyte antigen 6 complex locus D (*Ly6d*), keratin 19 (*Krt19*), Golgi membrane protein 1 (*Golm1*), and *Cd44,*[38] in non-tumoral liver parenchyma, that was completely normalized in HFD-fed mice treated with AAV-FGF21 vectors (Figures 3L–3P). All these results confirmed that treatment with AAV-FGF21 precluded progression from MASH to cirrhosis and HCC.

AAV-FGF21 treatment mediates reversal of WAT hypertrophy and inflammation

As observed with MASH development, 12 weeks after initiation of the HFD, increased fat accumulation in visceral and subcutaneous white adipose tissue (WAT) and brown adipose tissue (BAT), and increased weight of WAT and BAT depots were observed (Figures S5–S5D). As
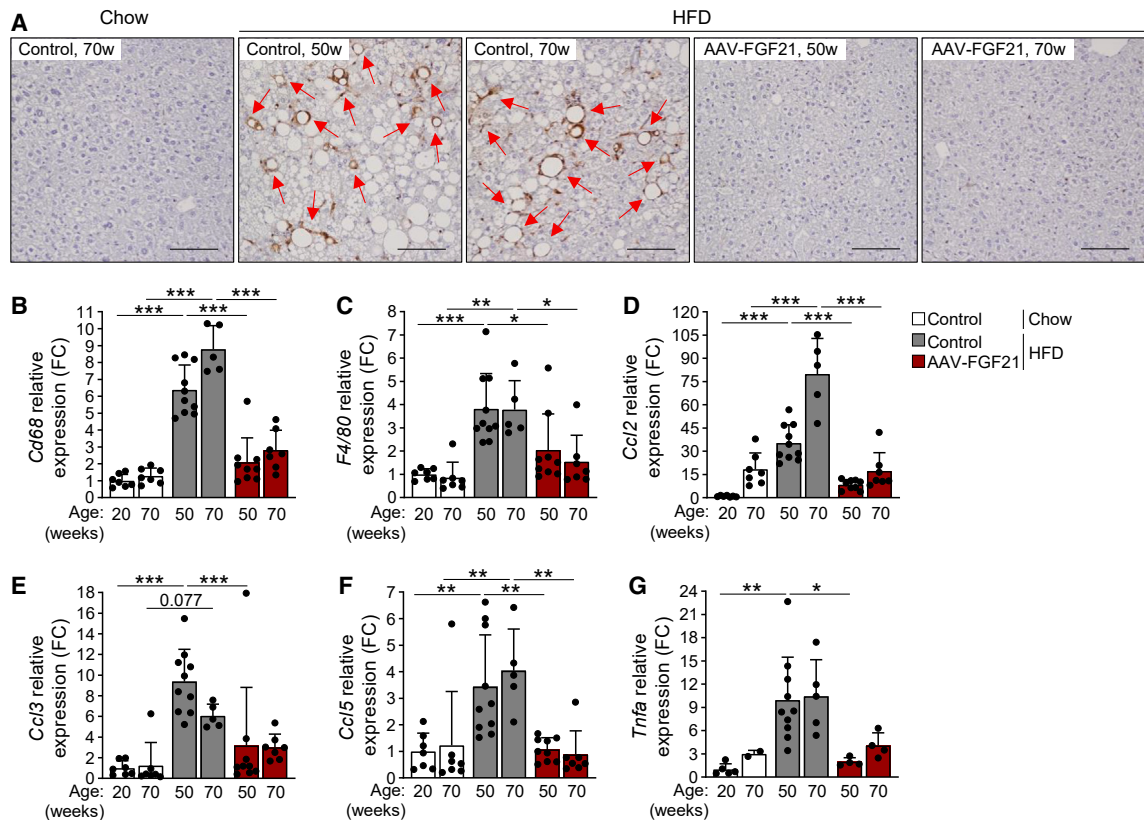
Figure 2. Treatment with AAV-FGF21 vectors reverts hepatic inflammation

(A) Representative images of liver sections immunostained against the macrophage marker MAC2. Red arrows indicate MAC2$^+$ cells. Scale bars, 100 μm. (B–G) Expression levels of the hepatic inflammatory markers *Cd68* (B), *F4/80* (C), *Ccl2* (D), *Ccl3* (E), *Ccl5* (F), and *Tnfa* (G) (n = 5–10/group). Data are presented as mean ± SD. *$p < 0.05$, **$p < 0.01$, ***$p < 0.001$ by one-way analysis of variance (ANOVA) with Bonferroni multiple comparison test. FC, fold change; w, weeks.

expected, this paralleled the severe macrophage inflammation of WAT and the markedly increased circulating levels of leptin, a key adipokine positively correlating with the amount of body fat that also exerts profibrogenic effects in the liver (Figures S5E–S5G).[39,40] Therefore, by the time of treatment with AAV-FGF21 vectors at age 28 weeks, HFD-fed animals had already developed severe adipose tissue alterations.

AAV-FGF21 gene therapy normalized the size of white adipocytes and weight of the epididimal, inguinal, mesenteric and retroperitoneal WAT depots (Figures 4A–4D and S5H–S5J). Moreover, in contrast to untreated HFD-fed mice, AAV-FGF21-treated animals also normalized serum leptin and showed a marked increase in levels of circulating adiponectin (Figures 4E and 4F). Adiponectin is known to exert anti-inflammatory, anti-steatotic, anti-fibrotic, and insulin-sensitizing effects[40] that will further contribute to FGF21 therapeutic benefits.

Adipocyte hypertrophy in non-treated HFD-fed mice resulted in severe macrophage inflammation of epididimal WAT (eWAT) demonstrated by increased presence of "crown-like" structures, which were

absent in mice treated with AAV-FGF21 vectors (Figure 4A). Moreover, the gene expression of the inflammatory markers *Cd68* and *F4/80* and of the soluble pro-inflammatory cytokine *Tnfa* was normalized (Figures 4G–4I). Similar observations were made in HFD-fed female mice treated with AAV-FGF21 vectors (Figures S6A–S6D). These results demonstrated that IM AAV-FGF21 gene therapy was able to revert WAT hypertrophy and inflammation.

AAV-FGF21 gene therapy increases energy expenditure

Despite a slight increase in food intake (Figure 5A), normalization of body weight in AAV-FGF21-treated HFD-fed mice was concordant with increased energy expenditure (Figure 5B), which likely resulted from both enhanced non-shivering thermogenesis and increased locomotor activity. Non-treated HFD-fed mice showed increased fat accumulation and weight of interscapular BAT (iBAT), which normalized in HFD-fed mice treated with AAV-FGF21 vectors (Figures 5C and 5D). Moreover, markedly increased gene expression of the thermogenic markers uncoupling protein 1 (*Ucp1*), cell death-inducing DNA fragmentation factor, α-subunit-like effector A (*Cidea*), and elongation of very long chain fatty acids (FEN1/Elo2, SUR4/Elo3, yeast)-like 3 (*Elovl3*) was also observed in the
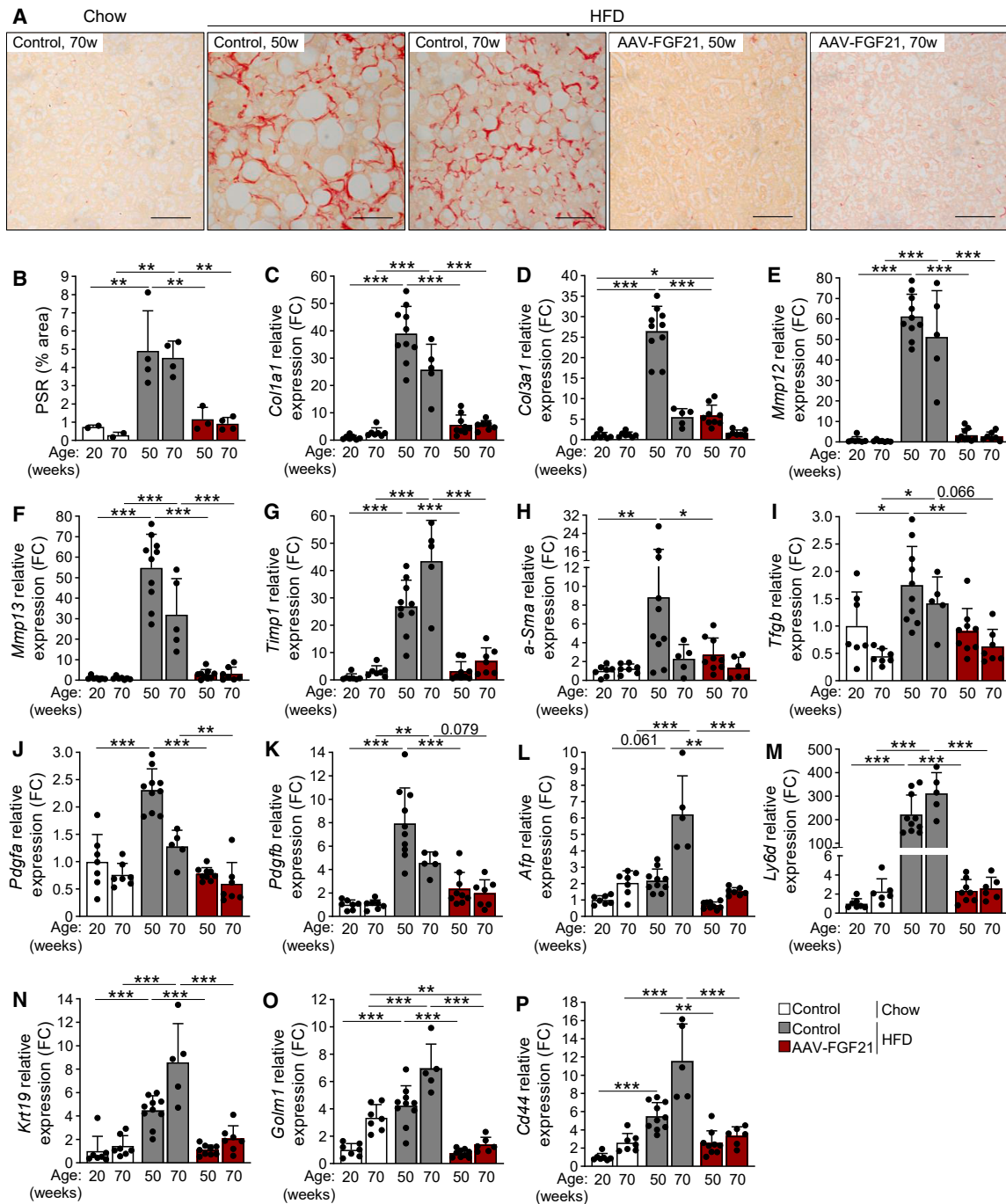
Figure 3. Muscle-derived FGF21 counteracts hepatic fibrosis and halts development of liver tumors

(A) Representative images of Picrosirius red (PSR) staining of liver sections showing liver fibrosis in red. Scale bars, 50 μm. (B) Histomorphometric quantitative assessment of liver fibrosis (PSR) (n = 2–4/group). (C and D) Expression levels of the liver fibrosis markers *Col1a1* (C) and *Col3a1* (D) (n = 5–10/group). (E–G) Expression levels of the genes involved in extracellular matrix deposition *Mmp12* (E), *Mmp13* (F), and *Timp1* (G) (n = 5–10/group). (H–K) Expression levels of the marker of activated hepatic stellate cells (HSCs) *a-Sma* (H) and key cytokines involved in HSCs activation *Tfgb* (I), *Pdgfa* (J), and *Pdgfb* (K) (n = 5–10/group). (L–P) Expression levels of the hepato-cellular carcinoma markers *Afp* (L), *Ly6d* (M), *Krt19* (N), *Golm1* (O), and *Cd44* (P), in non-tumoral liver parenchyma (n = 5–10/group). Data are presented as mean ± SD. *p < 0.05, **p < 0.01, ***p < 0.001 by one-way analysis of variance (ANOVA) with Bonferroni multiple comparison test. FC, fold change; w, weeks.
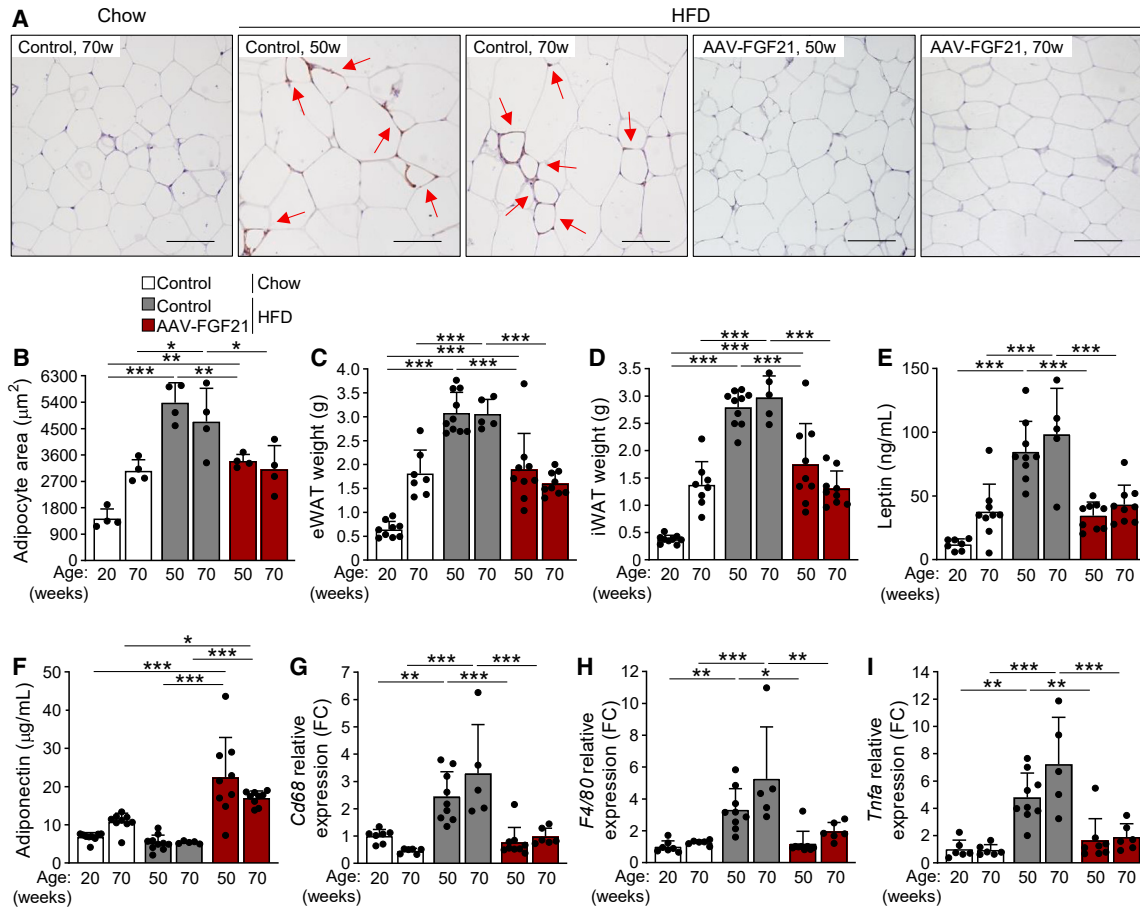
Figure 4. Reversal of WAT hypertrophy and inflammation by AAV1-FGF21 treatment

(A) Immunohistochemical analysis of MAC2 in eWAT sections. Red arrows indicate crown-like structures. Scale bars, 100 μm. (B) Morphometric analysis of the mean adipocyte area in eWAT (n = 4/group). (C and D) Weight of eWAT (C) and iWAT (D) depots (n = 5–10/group). (E and F) Serum leptin (E) and adiponectin (F) levels (n = 5–10/group). (G–I) Expression levels of the inflammatory markers *Cd68* (G), *F4/80* (H), and *Tnfa* (I) in eWAT (n = 5–10/group). Data are presented as mean ± SD; *$p < 0.05$, **$p < 0.01$, ***$p < 0.001$ by one-way analysis of variance (ANOVA) with Bonferroni multiple comparison test. FC, fold change; w, weeks.

AAV-FGF21-treated mice (Figures 5E–5G), consistent with enhancement of non-shivering thermogenesis. Similar results were obtained in HFD-fed female mice treated with FGF21-encoding vectors (Figures S6E–S6I).

The degree of spontaneous locomotor activity of 70-week-old HFD-fed mice treated with AAV-FGF21 was higher than that of age-matched control HFD- and chow-fed counterparts in the open-field test (Figure 5H). These mice traveled longer distance, moved at higher velocity for longer time, rested less, and spent more time doing fast and slow movements than untreated controls (Figures 5H–5N). Moreover, locomotor activity of AAV-FGF21-treated animals resembled that of non-treated young chow-fed animals (age 8 weeks) (Figures 5H–5N). This test also revealed that treatment with AAV-FGF21 reverted the anxiety observed in HFD-fed obese mice. Compared with their age-matched chow-fed counterparts, the time in the central zone was increased and the first entry in the center

decreased in AAV-FGF21 treated mice, which performed similarly to young lean animals (Figures 5O and 5P). Normal skeletal muscle weight and morphology and no signs of muscle pathology or inflammation were documented in AAV-treated animals (Figures S7A and S7B). Similar results were also obtained in AAV-FGF21-treated HFD-fed female mice (Figures S6J–S6O, S7C, and S7D).

Altogether, these results proved the pivotal role of AAV-derived increased circulating FGF21 levels to induce energy expenditure in obesogenic conditions.

Improved insulin sensitivity by AAV-FGF21 gene therapy

MASH and obesity are tightly associated with insulin resistance.[3,5,6] Hyperinsulinemia and mild hyperglycemia of non-treated HFD-fed male mice were normalized in AAV-FGF21-treated mice (Figures 6A, 6B, S7E, and S7F). To confirm the increased insulin sensitivity of FGF21-treated animals, an intraperitoneal insulin tolerance test
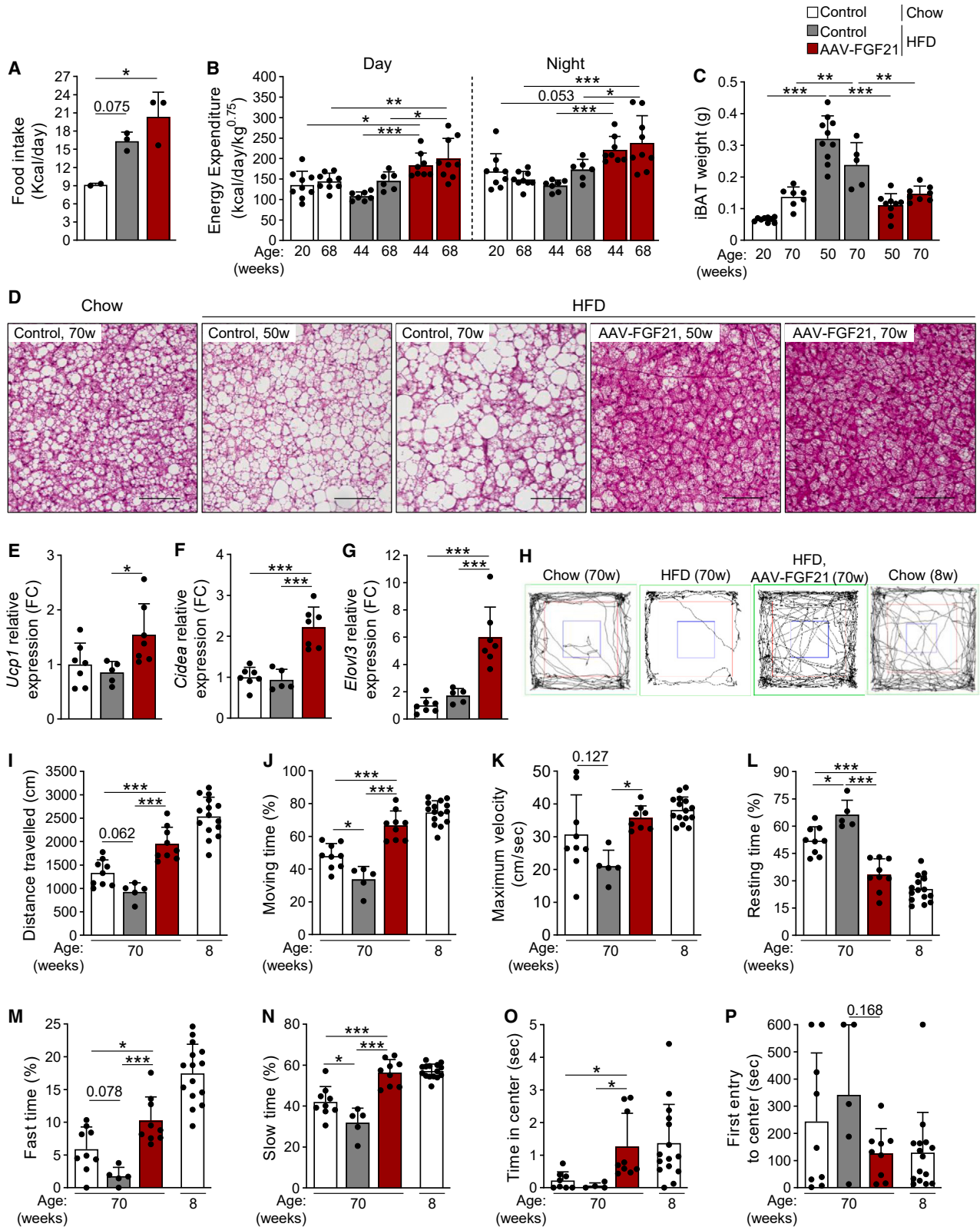
(legend on next page)

(ITT) was performed. As expected, HFD-fed mice showed loss of insulin sensitivity, whereas animals treated with AAV-FGF21 showed greater insulin sensitivity than chow-fed controls (Figure 6C). Similarly, treatment of HFD-fed female mice with AAV-FGF21 also resulted in improved insulin sensitivity (Figures S7G–S7I). Moreover, treatment with AAV-FGF21 counteracted the islet hyperplasia induced in insulin resistance conditions and decreased circulating levels of glucagon compared with HFD-fed control mice (Figures 6D–6F).

AAV-FGF21 treatment improves neuromuscular performance and cognition in HFD-fed mice

Obesity and insulin resistance are associated with impaired neuromuscular function, locomotor activity and coordination, anxiety-like behavior, and deficits in cognitive function in animal models and also in humans.[41–44] MASLD is also associated with cognitive impairment, worsening in patients with higher risk of liver fibrosis.[45] In this regard, treatment of HFD-fed obese mice with AAV-FGF21 vectors counteracted neuromuscular and cognitive decline (Figures 6G–6J). Treated mice displayed increased muscle strength and were able to stay longer on the accelerating rotarod than untreated HFD-fed counterparts, demonstrating improved coordination and balance (Figures 6G and 6H). Moreover, treated mice outperformed untreated HFD-fed mice in the novel object recognition test. These mice showed increased exploration time for the new object compared with HFD-fed non-treated mice and had a discrimination index equivalent to that of control chow-fed animals (Figures 6I and 6J), indicating prevention of memory loss. These therapeutic benefits may result from direct FGF21 effects on the brain, since native FGF21 can cross the blood-brain barrier.[46] HFD-fed female mice treated with AAV1-FGF21 vectors showed increased FGF21 content in the brain (Figure S7J), although these levels were very low compared with the circulating FGF21 serum levels. Therapeutic efficacy may also result from AAV-FGF21-mediated normalization of obesity, liver and adipose tissue inflammation, circulating leptin levels, and insulin resistance, whose alterations trigger detrimental effects on brain function.[47–49]

Treatment of Beagle dogs with AAV-FGF21 vectors

Toward the translation to the clinic of the AAV-FGF21-mediated gene therapy, healthy Beagle dogs (dog-1 and dog-2) were treated IM with 7×10^{12} vg/kg of AAV1 vectors encoding canine optimized FGF21 (AAV-coFGF21), which corresponded to the dose mediating full therapeutic efficacy in HFD-fed mice (3×10^{11} vg). Three untreated dogs were used as controls. Four months post-AAV adminis-

tration, biodistribution analysis indicated widespread coFGF21 gene expression and vector genome copy numbers in hindlimb skeletal muscles (Figures 7A and 7B). No transgene mRNA levels were observed in untreated skeletal muscles and liver (Figure 7A). Circulating biologically active FGF21 levels rose above baseline as early as 2 weeks after vector administration and remained high thereafter, reaching a plateau about 40 days post dosing (Figure 7C). The measured levels of canine FGF21 were likely underestimated given that basal FGF21 levels prior to AAV administration were undetectable using the iLite FGF21 assay, which was developed to assess human FGF21 levels. In agreement with increased biologically active AAV-derived FGF21 in bloodstream, mRNA levels of β-klotho also increased in the liver (Figure 7D). Dog-1 and dog-2 showed decreased serum triglycerides, and enhanced hepatic gene expression of key markers of β-oxidation, such as acyl-CoA dehydrogenase medium (ACADM) and long (ACADL) channel, and carnitine palmitoyl transferase 2 (CPT2) (Figures 7E–7G and S8A). Moreover, increased serum adiponectin levels and adiponectin gene expression in WAT were observed in the treated dogs (Figures 7H and 7I). WAT of these animals also showed presence of multilocular adipocytes and increased mRNA levels of thermogenic and β-oxidation markers (Figures 7J–7M and S8B–S8D).

Histological evaluation of AAV-FGF21-treated skeletal muscles revealed unaltered morphology and normal fiber size (Figures S8E and S8F). To further assess the safety of the approach and potential toxicities, animal health was periodically monitored through clinical, hematological, and biochemical examination. No clinically relevant deviations were observed in different parameters obtained throughout the 4-month follow-up, in agreement with the general health status of the animals (Tables S1 and S2). All these results highlighted that treatment with AAV-coFGF21 was safe and able to improve key metabolic parameters in large animals.

Analysis of circulating FGF21 levels in obese, T2D, and MASH patients

As a step forward toward clinical translation, circulating FGF21 levels were measured in approximately 500 highly obese, insulin-resistant, and T2D male and female patients. Two additional cohorts of 12 overweight and 46 lean subjects were analyzed as controls. Patient characteristics are provided in Table S3. Obese individuals were grouped by their body mass index (BMI, kg/m^2) in class I (BMI, 30–34.9), class II (BMI, 35–39.9), and class III (BMI, ≥40), according to the World Health Organization classification. From class I to III patients, a progressive increase in glycemic control markers, such as

---

Figure 5. AAV1-FGF21 treatment increases energy expenditure

(A) Food intake of male mice fed an HFD and treated with AAV1-FGF21 ($n = 2$–3 cages/group). (B) Energy expenditure was measured with an indirect open circuit calorimeter at different time points, during light and dark cycles ($n = 6$–10/group). (C) Interscapsular BAT (iBAT) weight of AAV-FGF21-treated male mice at different ages ($n = 5$–10/group). (D) Representative images of hematoxylin and eosin staining of iBAT sections. Scale bars, 100 μm. (E–G) Quantification of the expression of the non-shivering thermogenesis markers Ucp1 (E), Cidea (F), and Elovl3 (G) in iBAT at age 70 weeks ($n = 5$–10/group). (H) Representative tracks during the open field test of male mice at age 8 and 70 weeks. (I–P) Assessment of locomotor activity (I–N) and anxiety parameters (O and P) through the open-field test ($n = 5$–15/group). Data are presented as mean ± SD. *$p < 0.05$, **$p < 0.01$, ***$p < 0.001$ by one-way analysis of variance (ANOVA) with Tukey's (A, E–G, I–P) or Bonferroni (B and C) multiple comparison test. FC, fold change; w, weeks.
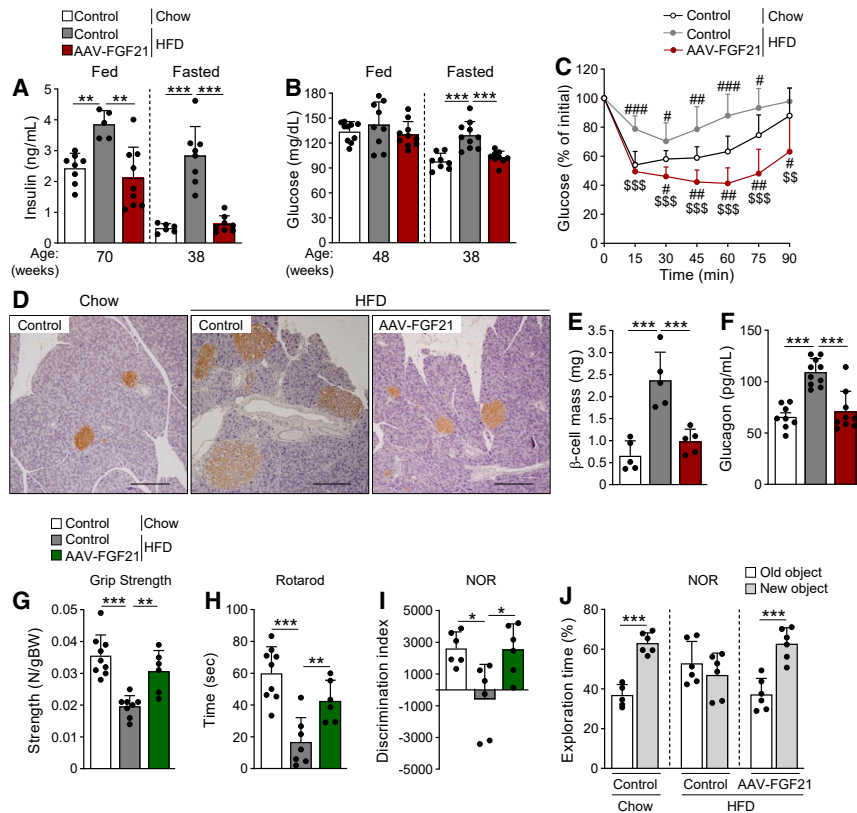
Figure 6. AAV1-FGF21 improves insulin sensitivity

(A) Fed and fasted serum insulin in male mice at age 70 and 38 weeks, respectively ($n = 5$–9/group). (B) Fed and fasted blood glucose in male mice at age 48 and 38 weeks, respectively ($n = 8$–10/group). (C) Insulin sensitivity was determined after an intraperitoneal insulin injection (0.75 units/kg) at age 59 weeks in male mice. Results were calculated as percentage of initial blood glucose levels ($n = 9$–10/group). (D) Representative images of insulin immunostaining in pancreas sections from AAV-FGF21-treated male mice. Scale bars, 500 μm. (E) Quantification of β cell mass in male mice at age 70 weeks ($n = 5$/group). (F) Fasted glucagon levels in male mice, 12 weeks post-AAV administration ($n = 8$–10/group). (G) Forelimb grip strength in female mice ($n = 6$–9/group). (H) Time before falling during the rotarod test performed in female mice ($n = 6$–9/group). (I and J) Discrimination index (I) and exploration time (J) during novel object recognition (NOR) test performed in female mice ($n = 6$/group). Data are presented as mean ± SD. $*p < 0.05$, $**p < 0.01$, $***p < 0.001$ by one-way analysis of variance (ANOVA) with Tukey's multiple comparison test (A, B and E–I) or Student's two-tailed t test (J). In (C), $\#p < 0.05$, $\#\#p < 0.01$, $\#\#\#p < 0.001$ versus chow-fed control group and $\$\$p < 0.01$, $\$\$\$p < 0.001$ versus HFD-fed control group by one-way analysis of variance (ANOVA) with Tukey's multiple comparison test. BW, body weight; N, Newtons.

fasting glucose, HbA1c, insulin, and HOMA-IR, in circulating triglycerides and in liver fibrosis markers (FLI, HIS, and TyG) was observed, consistent with MASH development (Table S3).

FGF21 circulating levels corresponding to 90% of healthy individuals ranged from 0 to 0.26 ng/mL (0–260 pg/mL) (Figure 8A). The determination of the normal range of FGF21 circulating levels in lean individuals was carried out including both men and women values. A very significant percentage (about 50%–80%) of T2D/obese class I to III patients also showed FGF21 levels in bloodstream comprised in this range (Figure 8A). Most of the remaining class II and III obese patients did not exceed the 2-fold limit of the normal range displayed by lean individuals (0.53 ng/mL) (Figure 8A). Similar observations were made in chow-fed mice compared with HFD-fed obese and insulin-resistant male and female mice, which showed a 2-fold increase in FGF21 circulating levels (Figures 1C and S2B). Higher FGF21 levels are consistently found in obese small and large animals.[50] Nevertheless, the present work demonstrates that obese mice were highly responsive to the AAV-FGF21-mediated gene therapy.

In this regard, treatment of male and female patients exhibiting circulating FGF21 levels comprised within the 2-fold limit of the normal range may also result in therapeutic benefit. From the cohort of 500 obese patients analyzed, only a limited number of subjects remained out of this range (Figure 8A). In addition, circulating FGF21 levels were also examined in a cohort of 20 biopsy-proven MASH patients

(Table S4). Similar to the results obtained in obese/T2D patients and independently of the liver fibrosis stage and BMI, most MASH patients had FGF21 levels within the 2-fold limit of the normal range of lean individuals (Figure 8B). Altogether, these results suggest that most obese, T2D, and MASH patients would be eligible for the AAV-FGF21 gene therapy.

DISCUSSION

In this study, we have demonstrated long-term MASH resolution in both HFD-fed and ob/ob male and female mice after one-time IM administration of a skeletal muscle-directed gene therapy to produce sustained circulating levels of native FGF21. Treatment with AAV-FGF21 vectors counteracted the key hepatic pathological alterations responsible for MASH development, i.e., steatosis-driven hepatocyte injury, macrophage-mediated inflammation, and HSC activation, which finally triggers fibrosis,[3] suggesting the therapeutic potential of this gene therapy to revert advanced MASH in patients. Moreover, treatment of HFD-fed mice with AAV-FGF21 vectors reverted hepatic fibrosis and precluded progression of MASH toward development of liver tumors and the induction of HCC markers in non-tumoral liver parenchyma, common features of long-term HFD feeding.[37] In agreement, FGF21 deficiency in T2D and obese mice has been associated with hepatic cancerous hyperproliferation, aberrant oncogene and tumor suppressor signaling and increased incidence of HCC.[51–53] Moreover, overexpression of FGF21 specifically in the liver or treatment with native FGF21 also reduced chemically induced tumors.[54,55]
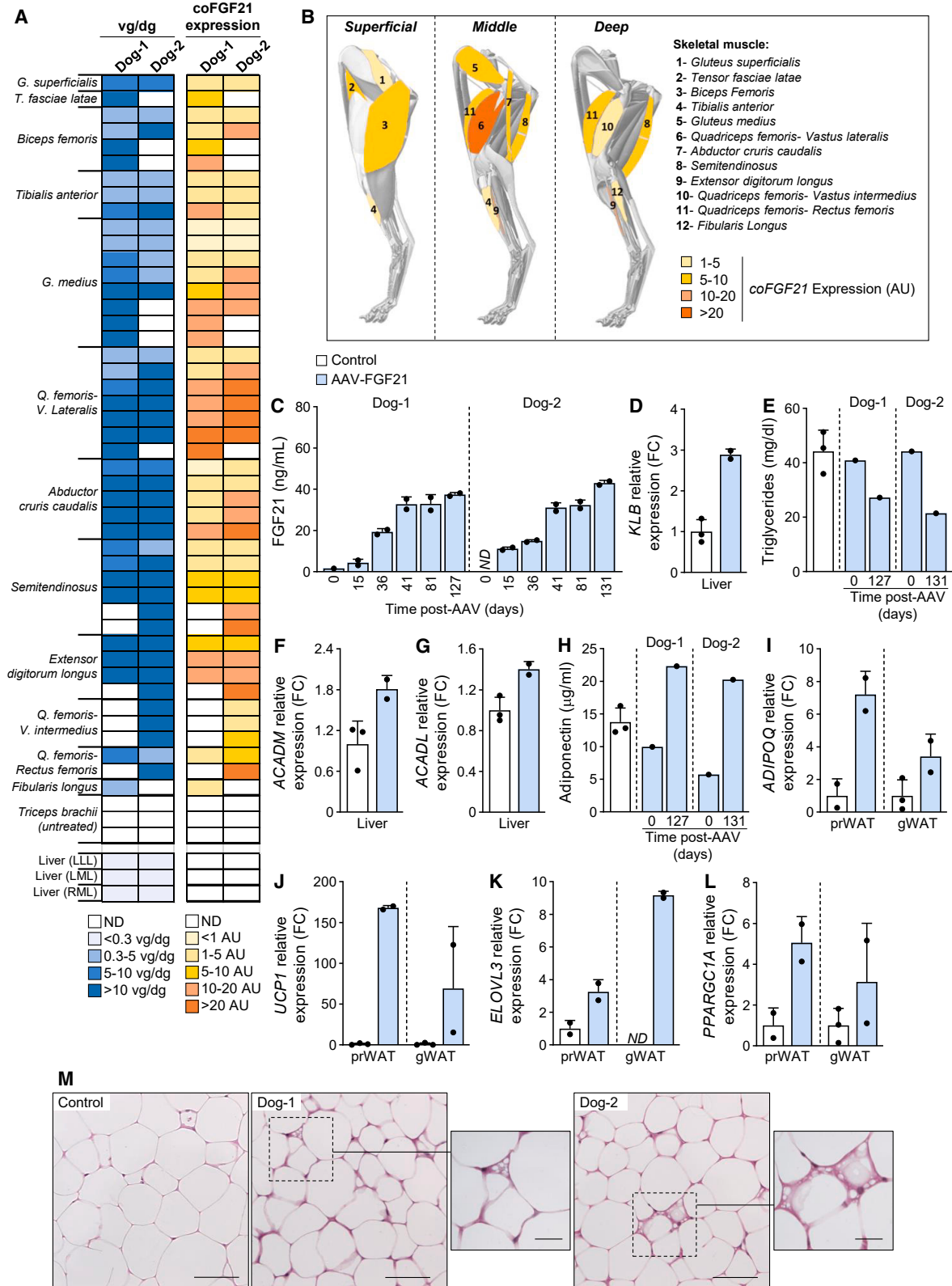
Toward the translation to the clinic of the AAV-FGF21-mediated gene therapy, scale-up of muscular gene transfer to healthy dogs was shown to be safe and resulted in secretion of biologically active FGF21 in blood. AAV-derived FGF21 mediated key metabolic effects, including decreased circulating TG and increased adiponectin levels. Serum adiponectin, an anti-inflammatory, anti-steatotic, anti-fibrotic, and insulin-sensitizing adipokine,[40] is consistently elevated in animals and humans treated with FGF21.[20] Indeed, adiponectin is presently considered a clinical biomarker for FGF21 signaling pathway activation.[20]

Recent studies have revealed that treatment with FGF21 engineered proteins (FGF21 analogs/mimetics) also reduced liver steatosis, inflammation, and fibrosis in preclinical studies in small and large animal models and in patients in multiple mid-stage clinical trials.[19,20,56–58] Nevertheless, FGF21 analogs/mimetics require weekly to biweekly subcutaneous administrations to mediate clinical benefit, which may be uncomfortable for patients and compromise treatment compliance. In this regard, despite weight loss, up to half of patients treated with incretin-based obesity medications have discontinued treatment after 1 year.[59–62] In contrast, one-time IM AAV-FGF21 administration may eliminate compliance issues associated with complex medication regimens and has the potential to deliver multiyear efficacy in the setting of MASH, a chronic lifelong disease. A single IM administration of AAV1 vectors encoding for insulin and glucokinase to diabetic dogs resulted in successful, multiyear (>8 years) control of glycemia without the need of supplementation with exogenous insulin.[16,17] In the first AAV approved human gene therapy—alipogene tiparvovec for the treatment of familial lipoprotein lipase deficiency—durability of response up to 6 years upon IM delivery of therapeutic AAV1 vectors has been reported.[13] Similarly, muscle-directed AAV1-based therapy for α-1-antitrypsin deficiency has thus far demonstrated stable transgene expression at 5 years after vector dosing.[14] In hemophilia B, factor IX (FIX) expression has been detected up to 10 years post IM AAV administration in human skeletal muscle.[15]

Furthermore, AAV-derived native FGF21 avoids unnatural modifications incorporated into FGF21 analogs to extend half-life, which prevents the development of immune responses associated with the administration of exogenous proteins and may support better tissue distribution and receptor binding. Humoral responses (including anti-drug antibodies and neutralizing antibodies) have been observed shortly after administration of FGF21 analogs/mimetics to non-human primates and humans.[63–73]

Continuous expression of AAV-derived native FGF21 also delivers a steady level of the protein, to avoid peak-to-trough pharmacokinetic variability associated with recombinant analog products that require frequent injections, which may lead to better treatment outcomes. In this regard, AAV-mediated gene therapy has already demonstrated superior therapeutic potential in comparison with administration of recombinant proteins in several severe diseases. A hemophilia B clinical trial demonstrated absence of bleedings after administration of therapeutic AAV vector in 9 out of 10 enrolled patients, whereas treatment with recombinant FIX, prior to vector delivery, failed to prevent bleedings in all the participants.[74] Similarly, AAV-based gene therapy resulted in enhanced pharmacokinetics and uptake of acid α-glucosidase in peripheral tissues and improved respiratory function compared with enzyme replacement therapy in Pompe mice.[75,76] In addition, consistent concentration of AAV-derived native FGF21 protein may also limit C_{max}-mediated gastrointestinal issues observed in clinical trials with FGF21 analogs/mimetics.[68,69,71–73,77,78] Therefore, our AAV-FGF21 gene therapy may have seminal benefits in comparison with FGF21 mimetics/analogs.

In summary, this study provides strong evidence of the feasibility, and non-clinical durability, safety, and efficacy of the IM AAV1-FGF21-based gene therapy against MASH, T2D, and obesity. Our results support the clinical translation of the approach but further nonclinical studies in larger animals are needed to determine optimal doses in the clinical trials. Moreover, safety and efficacy in humans should be evaluated during the FIH studies where long-term patient monitoring, up to 15 years (FDA), common in gene therapy trials, should be implemented. Altogether, this study highlights that the muscle-directed AAV1-FGF21-based strategy may be a major breakthrough in the treatment of MASH patients and create a therapeutic avenue for the treatment of other metabolic diseases and related comorbidities that impact millions of people worldwide.

MATERIAL AND METHODS
Animals
C57Bl/6JOlaHsd and B6.V-Lep^{ob}/OlaHsd (ob/ob) male and female mice were used. Mice were kept in a specific pathogen-free facility

Figure 7. AAV1-FGF21 biodistribution and biological activity in dogs
Healthy Beagle dogs (dog-1 and dog-2) were treated with 7×10^{12} vg/kg of AAV1-canine optimized FGF21 and followed up for 4 months. (A) Vector genome copy number (left panel, blue) and canine optimize *FGF21* (*coFGF21*) expression (right panel, orange) were analyzed in tissue punches from multiple regions of the skeletal muscle and the liver obtained during necropsy of dogs. (B) Schematic representation indicating the mean *coFGF21* expression in hindlimb skeletal muscles. Image courtesy of IMAIOS (Micheau A, Hoa D, e-Anatomy, www.imaios.com, https://doi.org/10.37019/e-anatomy). (C) Levels of biologically active FGF21 in fasted conditions measured using a cell-based reporter gene assay (iLite). (D) Hepatic expression levels of *KLB* (n = 2–3/group). (E) Serum triglyceride levels pre-AAV and 4 months post-AAV (n = 1–3). (F and G) Hepatic expression levels of *ACADM* (F) and *ACADL* (G) (n = 2–3/group). (H) Serum adiponectin levels pre-AAV and 4 months post-AAV (n = 1–3). (I–L) Quantification of *ADIPOQ* (I), *UCP1* (J), *ELOVL3* (K), and PPARGC1A (L) expression in perirenal (prWAT) and gluteal WAT (gWAT) (n = 2–3/group). (M) Representative images of the hematoxylin and eosin staining of prWAT sections. Insets show multilocular adipocytes in prWAT of AAV-FGF21-treated dogs. Scale bars, 100 μm. Inset scale bars, 25 μm. Data are presented as mean ± SD. Data were analyzed using a Mann-Whitney two-tailed test. coFGF21, canine optimized FGF21; ND, non-detected; vg/dg, vector genomes/diploid genome; AU, arbitrary units; FC, fold change; G, gluteus; T, tensor; Q, quadriceps; V, vastus; LLL, left lateral lobe; LML, left medial lobe; RML, right medial lobe.
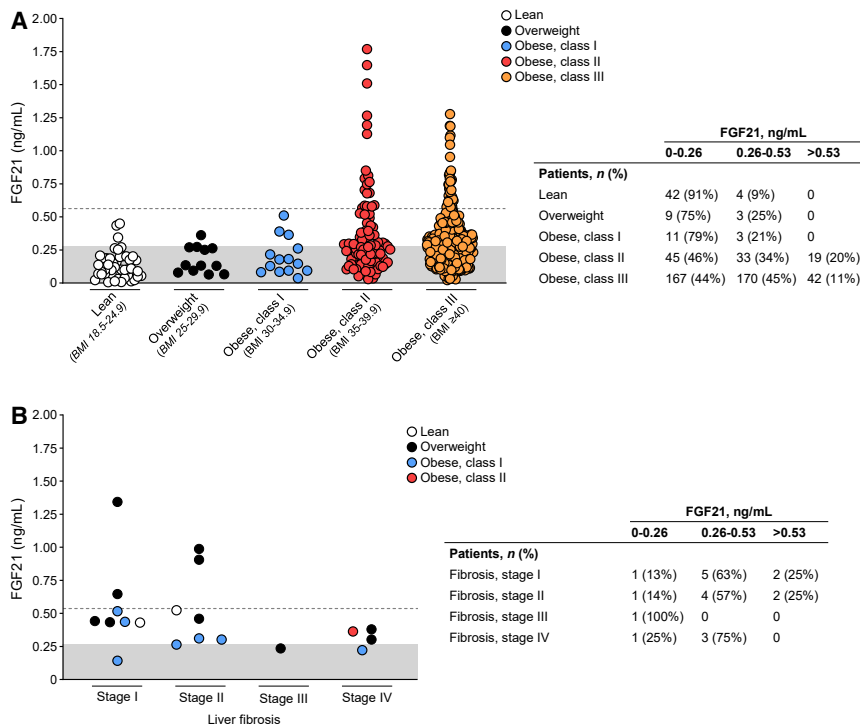
Figure 8. FGF21 circulating levels in human patients
(A and B) Serum FGF21 levels were measured in a cohort of 46 lean and 12 overweight individuals and in a cohort of approximately 500 highly obese and insulin-resistant patients, grouped by body mass index (BMI) (A) and in a cohort of 20 biopsy-proven MASH patients and grouped by fibrosis stage (B). Gray bar indicates FGF21 circulating levels corresponding to 90% of healthy individuals (0–0.26 ng/mL). The 2-fold limit of the normal range displayed by lean individuals (0.53 ng/mL) is indicated with the dashed line. n, number of individuals.

Participants gave their written informed consent, which was validated by the Ethical Review Board.

Recombinant AAV vectors

AAV expression cassettes were obtained by cloning, between the ITRs of AAV2, the murine, canine, or human codon-optimized FGF21 coding sequence under the control of the CMV promoter. Single-stranded AAV1 vectors were produced by triple transfection in HEK293 cells and purified using a double CsCl gradient-based purification protocol that renders vector preps of high purity with negligible amounts of empty capsids.[79] Viral genome titers were determined by PicoGreen (Quant-iT PicoGreen dsDNA assay kit, Invitrogen), using phage lambda DNA to generate the standard curve (titers: AAV1-FGF21, 5.44×10^{13} vg/mL, and AAV1-coFGF21, 6.51×10^{13} vg/mL). The same batch of AAV1-FGF21 vectors was used for all the mouse experimental work. Similarly, all the treated dogs were IM administered with the same batch of AAV1-coFGF21 vectors.

AAV-FGF21 IM administration

Mice were anesthetized with an intraperitoneal injection of ketamine (100 mg/kg) and xylazine (10 mg/kg). Hindlimbs were shaved, and AAV vectors were IM administered in a volume of 180 μL divided into six injection sites (5×10^{10} vg in a volume of 30 μL per site) distributed between quadriceps, gastrocnemius, and tibialis cranialis of each hindlimb (one site per skeletal muscle). AAV delivery in dogs was performed as described previously.[16,17] In brief, anesthesia started with premedication with 0.2 mg/kg IM butorphanol and 0.025 mg/kg aceopromazine. Thirty minutes later, induction was performed with 4 mg/kg propofol (Propovet, B. Braun) and 0.5 mg/kg diazepam (Valium, F. Hoffmann-La Roche) administered intravenously. After endotracheal intubation, anesthesia was maintained by inhalation of 2% isoflurane (IsoVet, B. Braun) in 100% oxygen. AAV vectors were delivered manually to a total of 33–40 sites (1×10^{12} vg in a volume of 400 μL per site) in each hindlimb, distributed on the lateral aspect of the thigh (isquiotibialis muscles) (with a five-prong needle syringe [Meso-relle, Biotekne SRL]) and the tibialis anterior muscle (single point injections). Throughout the procedure,

at the Center of Animal Biotechnology and Gene Therapy, Universitat Autònoma Barcelona (UAB), and maintained under a light-dark cycle of 12 h at 22°C. Mice were fed ad libitum with a standard diet (2018S Teklad Global Diets, Envigo) or a HFD (TD.88137 Teklad, Envigo). When stated, mice were fasted for 16 h. For tissue sampling, mice were anesthetized with inhalational anesthetic isoflurane (IsoFlo, Abbott laboratories) and decapitated. Tissues of interest were excised and kept at −80°C or in formalin until analysis. Male Beagle dogs were purchased from Isoquimen S.L. and housed at Servei de Granges i Camps Experimentals of the UAB. Animals were fed once daily at 9:00 a.m.with dry food (Elite Nutrition, Nestle). Dogs' health was monitored through clinical, hematological, and biochemical examination at the UAB Veterinary Clinical Hospital and sacrificed by administration of a lethal dose of pentobarbital. Animal care and experimental procedures were approved by the Ethics Committee for Animal and Human Experimentation of the UAB (protocol numbers P2/3944 (9829) and P1/5408 (11391)).

Human samples

Human samples were provided by Parc Taulí Hospital Universitari (Sabadell, Barcelona, Spain) to determine FGF21 and insulin levels. Blood samples were collected after overnight fasting. All samples were centrifuged, fractionated and serum stored at −80°C until further analysis. Patients' clinical data and biochemical parameters were provided by the hospital. The study protocol was approved by the hospital Ethical Committee (Comité de Ética de la Investigación con medicamentos of Parc Taulí [study number MR2019593]) and conducted according to the principles of the Declaration of Helsinki.

temperature, cardiac and respiratory frequency, arterial pressure, pulse, and electrocardiography were monitored using a multifunctional patient Vet Care monitor (B. Braun Medical).

ITT

For ITT, insulin (Humulin Regular; Eli Lilly) was injected intraperitoneally to fed mice at a dose of 0.75 IU/kg body weight. Glycemia was measured in tail vein blood samples at the indicated time points.

Indirect calorimetry

An indirect open circuit calorimeter (Oxylet, Panlab) was used to monitor O_2 consumption and CO_2 production. Mice were individualized and acclimated to the metabolic chambers for 24 h, and data were collected in each cage for 5 min, every 45 min, for 24 h, during the light and dark cycles and adjusted by body weight.

Open-field test

The open-field test was performed between 9:00 a.m. and 1:00 p.m. as reported previously.[80] In brief, animals were placed in a corner of a square area surrounded by high white walls (45 × 45 × 40 cm) and motor and exploratory activities were evaluated during the first 6 min using a video tracking system (SMART Junior, Panlab).

Grip strength test

A grip strength test meter (Panlab) was used to assess forelimb grip strength. The grip strength meter was positioned horizontally, and mice were held by the tail and lowered toward the apparatus. Animals were allowed to grasp the metal bar with their front paws and were then pulled backward in the horizontal plane. The force applied to the bar just before it lost grip was recorded as the peak tension. The average of three trials was analyzed.

Rotarod test

Mice were placed on a rotating rod (Panlab), spinning at 4 rpm. Lane width, 50 mm; rod diameter, 30 mm. Once stabilized, mice were subjected to an incrementally increasing speed from 4 to 40 rpm in 5 min. The first day of the experiment was used to train the animals in the use of the device. Each animal underwent 3 trials. The length of time that the mice managed to remain on the rod was recorded. Then, animals underwent 1 day resting and the third day, mice took 3 more trials on the rod. The average of 3 trials was analyzed.

Novel object recognition test

The novel object recognition tests were conducted in the open field box.[81] Open-field test was used to acclimatize the mice to the box. The next day, to conduct the first trial, two identical objects (A and B) were placed in the upper right and upper left quadrants of the box, and then mice were placed backward to both objects. After 10 min of exploration, mice were removed from the box, and allowed a 10 min break. In the second trial, one of the identical objects (A and B) was replaced with object C (new object). Mice were then put back into the box for a further 10 min of exploration. The amount of time animals spent exploring the novel object was recorded and evaluated

using a video tracking system (SMART Junior, Panlab). Mice with exploration times for both objects shorter than 5 s, either during the first or the second trial, were excluded from analysis, as it cannot be confirmed that they spent enough time exploring to learn/discriminate the objects. The evaluation of novel object recognition test memory was expressed as a percentage of the discrimination ratio calculated according to the following formula: discrimination ratio (%) = (N − F)/(N + F) × 100%, where N represents the time spent in exploring the new object and F represents the time spent in exploring the same object.

Hormone and metabolite assays

Hepatic triglyceride and cholesterol contents were determined by chloroform/methanol (2:1 vol/vol) extraction of total lipids.[82] Triglycerides, cholesterol, and ALT were quantified spectrophotometrically using an enzymatic assay (Horiba-ABX) in a Pentra 400 Analyzer (Horiba-ABX). Glycemia was determined using a Glucometer Elite (Bayer). The Mouse/Rat FGF-21 ELISA kit (MF2100, R&D Systems) was used to determine FGF21 levels in serum and brain. Brain samples (cerebellum) were homogenized with T-PER buffer (Thermo Fisher Scientific) using a sonicator (VC130PB, Sonics & Materials). Buffer was supplemented with protease inhibitors (Complete, Roche) and phosphatase inhibitors (orthovanadate). Once homogenized samples were centrifuged at 10,000 × g during 10 min at 4°C and supernatant was kept at −80°C until analysis. Serum insulin, glucagon, adiponectin, and leptin levels in mice were determined using a Rat Insulin ELISA kit (90010, Crystal Chem), glucagon radioimmunoassay (#GL-32K, EMD Millipore), a Mouse Adiponectin ELISA kit (80569, Crystal Chem), and a Mouse Leptin ELISA kit (90030, Crystal Chem), respectively. Serum insulin and FGF21 levels in human samples were determined using a Human insulin ELISA kit (90095, Crystal Chem) and a Human FGF-21 ELISA kit (DF2100, R&D Systems). Canine adiponectin in serum was measured using the Human adiponectin ELISA High sensitivity kit (RD191023100, BioVendor Group), which has been previously validated for reliable measurement of canine adiponectin.[83,84] Serum FGF21 levels in dogs remained undetectable when measured with four different canine FGF21 ELISAs (E08F0016, Blue Gene; MBS028669, MyBiosource; ABIN1053687, Antibodies-online; KT-100218, Kamiya Biomedical Company). Experiments performed *in vitro* demonstrated that canine FGF21 activity in the cell medium could be identified in a manner similar to that of human FGF21 using the cell-based reporter gene assay iLite FGF21 assay ready cells (BM3071, Svar Life Science) (Figure S9). Therefore, biologically active canine FGF21 in circulation pre- and post-AAV treatment was evaluated using this assay.

Clinical laboratory and hematological parameters in dogs

General lab parameters were measured by spectrophotometry with a Cobas Mira Analyzer (Roche) at the Servei de Bioquímica Clínica Veterinària (Veterinary School, UAB). Hematological parameters were determined using an SCIL VetABC haematology analyzer by the Servei d'Hematologia Clínica Veterinària (Veterinary School, UAB).

RNA analysis

Total RNA was obtained from different tissues using isolation reagent (Tripure, Roche, and QIAzol, QIAGEN) and an RNeasy Minikit (QIAGEN) and treated with DNase I (QIAGEN). For gene expression quantification, 1 μg of RNA was reverse-transcribed using the Transcriptor First Strand cDNA Synthesis kit (Roche). Real-time quantitative PCR was performed in a Lightcycler (Roche) using the Lightcycler 480 SyBr Green I Master Mix (Roche) and the primers in Table S5 or Taqman Probes Master (Roche) and the primers and probes listed in Table S6. Data were normalized to Rplp0 expression.

Vector genome copy number

Dog skeletal muscle and liver samples were digested overnight (ON) at 56°C in 300 μL of Tissue Lysis Solution with Proteinase K (0.2 mg/mL). Total DNA was isolated from supernatants using a MasterPure DNA Purification Kit (Lucigen). DNA was extracted following the manufacturer's instructions and resuspended in distilled water and quantified using a NanoDrop ND-1000 spectrophotometer (Thermo Fisher Scientific). Vector genome copy number in 40 ng of total DNA was determined by quantitative PCR using LightCycler 480 Probes Master (Roche) and primers and probes specific for canine optimized FGF21 coding sequences listed in Table S6. A reference standard curve was built from serial dilutions of linearized plasmid bearing the CMV promoter and optimized canine FGF21 cDNA spiked into 20 ng/μL of non-transduced dog genomic DNA.

Histology and immunohistochemistry

Tissues were fixed for 12–24 h in 10% formalin, embedded in paraffin, and sectioned. Sections were incubated overnight at 4°C with rat anti-MAC2 (1:50, CL8942AP, Cedarlane), guinea pig anti-insulin (1:100, I-8510, Sigma-Aldrich), rabbit anti-laminin (1:200, Ab11575, Abcam), or anti-α-fetoprotein (1:100, Ab46799, Abcam). Biotinylated rabbit anti-rat (1:300, E0467, Dako), rabbit anti-guinea pig coupled to peroxidase (1:300, P0141, Dako), goat anti-rabbit (1:100, 31820, Invitrogen), or goat anti-rabbit (Alexa Fluor 488-conjugated) (1:100, A11008, Molecular probes) were used as secondary antibodies. The ABC peroxidase kit (Pierce) was used for immunodetection, and sections were counterstained in Mayer's hematoxylin. Hoechst (B2261, Sigma-Aldrich) was used for nuclear counterstaining of fluorescent specimens. Hepatic fibrosis was assessed by the percentage of the PSR-positive area quantified in 10 randomly selected ×100 fields per liver section.[85] Morphometric analysis of adipocyte size was performed in eWAT sections stained with hematoxylin and eosin.[86] β Cell mass was determined in insulin-stained pancreas sections as described previously.[87]

Statistical analysis and data processing

Sample size determination was based on previous experience with similar studies. For mouse studies, randomization was performed using GraphPad QuickCalcs to allocate mice in each group. In addition, we tested that the mean body weight and the mean glycemia were statistically not different for each experimental group prior to assignment to diet and/or treatment groups. Control mice were matched by sex. Furthermore, each experimental group was caged separately to avoid any caging effects. Statistics were calculated using GraphPad Prism. Data points beyond 2 standard deviations (SD) were considered extreme values and were therefore excluded from the analysis. Data are presented as mean ± SD. Statistical significance was calculated using a one-way ANOVA with Tukey's, Dunnett's, or Bonferroni multiple comparison test, Student's two-tailed t test and Mann-Whitney two-tailed test. For comparisons involving several time points, ANOVA Bonferroni test was used to compare the different groups. Differences were considered significant when $p < 0.05$.

DATA AND CODE AVAILABILITY

All data supporting the findings of this study are available within the paper and its supplemental information.

AUTHOR CONTRIBUTIONS

V.J. and F.B. conceived the project, designed and supervised experiments, and wrote and edited the manuscript. V.J., V. Sacristan, and C.J. generated reagents and performed experiments. X.L. generated reagents. M.L.J., E.C., S. Marcó, S. Muñoz, M.G., I.G., I.E., A.R., G.E., V. Sanchez, L.V., A. Casellas, T.F., J.R., M.M., A. Carretero, M.P., M.N., A.A., X.M., and S.A. performed experiments. M.V. and A. Caixàs contributed to analysis of human clinical data. V.J., V. Sacristan, C.J., and F.B. analyzed the data. V.J., V. Sacristan, S.F., and F.B. contributed to discussion and reviewed/edited the manuscript.

DECLARATION OF INTERESTS

V.J., V. Sacristan, C.J., I.E., I.G., A.R., and F.B. are co-inventors on patent applications for the use of AAV vectors for the treatment of metabolic diseases. F.B. is member of the scientific advisory board of Kriya Therapeutics.

SUPPLEMENTAL INFORMATION

Supplemental information can be found online at https://doi.org/10.1016/j.ymthe.2024.10.023.

REFERENCES

1. Dufour, J.-F., Scherer, R., Balp, M.-M., McKenna, S.J., Janssens, N., Lopez, P., and Pedrosa, M. (2021). The global epidemiology of nonalcoholic steatohepatitis (NASH) and associated risk factors–A targeted literature review. Endocr. Metab. Sci. 3, 100089.

2. Rinella, M.E., Lazarus, J.V., Ratziu, V., Francque, S.M., Sanyal, A.J., Kanwal, F., Romero, D., Abdelmalek, M.F., Anstee, Q.M., Arab, J.P., et al. (2023). A multisociety Delphi consensus statement on new fatty liver disease nomenclature. J. Hepatol. 79, 1542–1556.

3. Filipovic, B., Lukic, S., Mijac, D., Marjanovic-Haljilji, M., Vojnovic, M., Bogdanovic, J., Glisic, T., Filipovic, N., Al Kiswani, J., Djokovic, A., et al. (2021). The New Therapeutic Approaches in the Treatment of Non-Alcoholic Fatty Liver Disease. Int. J. Mol. Sci. 22, 13219.

4. Hagström, H., Nasr, P., Ekstedt, M., Hammar, U., Stål, P., Hultcrantz, R., and Kechagias, S. (2017). Fibrosis stage but not NASH predicts mortality and time to development of severe liver disease in biopsy-proven NAFLD. J. Hepatol. 67, 1265–1273.

5. Jarvis, H., Craig, D., Barker, R., Spiers, G., Stow, D., Anstee, Q.M., and Hanratty, B. (2020). Metabolic risk factors and incident advanced liver disease in non-alcoholic fatty liver disease (NAFLD): A systematic review and meta-analysis of population-based observational studies. PLoS Med. 17, e1003100.

6. Bian, H., Zhu, X., Xia, M., Yan, H., Chang, X., Hu, X., Pan, B., Guo, W., Li, X., and Gao, X. (2020). Impact of type 2 diabetes on nonalcoholic steatohepatitis and advanced fibrosis in patients with nonalcoholic fatty liver disease. Endocr. Pract. 26, 444–453.

7. O'Hara, J., Finnegan, A., Dhillon, H., Ruiz-Casas, L., Pedra, G., Franks, B., Morgan, G., Hebditch, V., Jönsson, B., Mabhala, M., et al. (2020). Cost of non-alcoholic steatohepatitis in Europe and the USA: The GAIN study. JHEP Rep. 2, 100142.

8. Kingwell, K. (2024). NASH field celebrates 'hurrah moment' with a first FDA drug approval for the liver disease. Nat. Rev. Drug Discov. 23, 235–237. https://doi.org/10.1038/d41573-024-00051-1.

9. https://www.fda.gov/news-events/press-announcements/fda-approves-first-treatment-patients-liver-scarring-due-fatty-liver-disease.

10. Harrison, S.A., Bedossa, P., Guy, C.D., Schattenberg, J.M., Loomba, R., Taub, R., Labriola, D., Moussa, S.E., Neff, G.W., Rinella, M.E., et al. (2024). A Phase 3, Randomized, Controlled Trial of Resmetirom in NASH with Liver Fibrosis. N. Engl. J. Med. 390, 497–509.

11. Wang, D., Tai, P.W.L., and Gao, G. (2019). Adeno-associated virus vector as a platform for gene therapy delivery. Nat. Rev. Drug Discov. 18, 358–378.

12. Mendell, J.R., Al-Zaidy, S.A., Rodino-Klapac, L.R., Goodspeed, K., Gray, S.J., Kay, C.N., Boye, S.L., Boye, S.E., George, L.A., Salabarria, S., et al. (2021). Current Clinical Applications of In Vivo Gene Therapy with AAVs. Mol. Ther. 29, 464–488.

13. Gaudet, D., Stroes, E.S., Méthot, J., Brisson, D., Tremblay, K., Bernelot Moens, S.J., Iotti, G., Rastelletti, I., Ardigo, D., Corzo, D., et al. (2016). Long-Term Retrospective Analysis of Gene Therapy with Alipogene Tiparvovec and Its Effect on Lipoprotein Lipase Deficiency-Induced Pancreatitis. Hum. Gene Ther. 27, 916–925.

14. Mueller, C., Gernoux, G., Gruntman, A.M., Borel, F., Reeves, E.P., Calcedo, R., Rouhani, F.N., Yachnis, A., Humphries, M., Campbell-Thompson, M., et al. (2017). 5 Year Expression and Neutrophil Defect Repair after Gene Therapy in Alpha-1 Antitrypsin Deficiency. Mol. Ther. 25, 1387–1394.

15. Buchlis, G., Podsakoff, G.M., Radu, A., Hawk, S.M., Flake, A.W., Mingozzi, F., and High, K.A. (2012). Factor IX expression in skeletal muscle of a severe hemophilia B patient 10 years after AAV-mediated gene transfer. Blood 119, 3038–3041.

16. Jaén, M.L., Vilà, L., Elias, I., Jimenez, V., Rodó, J., Maggioni, L., Ruiz-de Gopegui, R., Garcia, M., Muñoz, S., Callejas, D., et al. (2017). Long-Term Efficacy and Safety of Insulin and Glucokinase Gene Therapy for Diabetes: 8-Year Follow-Up in Dogs. Mol. Ther. Methods Clin. Dev. 6, 1–7.

17. Callejas, D., Mann, C.J., Ayuso, E., Lage, R., Grifoll, I., Roca, C., Andaluz, A., Ruiz-de Gopegui, R., Montané, J., Muñoz, S., et al. (2013). Treatment of diabetes and long-term survival after insulin and glucokinase gene therapy. Diabetes 62, 1718–1729.

18. Li, S., Zou, T., Chen, J., Li, J., and You, J. (2024). Fibroblast growth factor 21: An emerging pleiotropic regulator of lipid metabolism and the metabolic network. Genes Dis. 11, 101064.

19. Raptis, D.D., Mantzoros, C.S., and Polyzos, S.A. (2023). Fibroblast Growth Factor-21 as a Potential Therapeutic Target of Nonalcoholic Fatty Liver Disease. Ther. Clin. Risk Manag. 19, 77–96.

20. Talukdar, S., and Kharitonenkov, A. (2021). FGF19 and FGF21: In NASH we trust. Mol. Metab. 46, 101152.

21. Jimenez, V., Jambrina, C., Casana, E., Sacristan, V., Muñoz, S., Darriba, S., Rodó, J., Mallol, C., Garcia, M., León, X., et al. (2018). FGF21 gene therapy as treatment for obesity and insulin resistance. EMBO Mol. Med. 10, e8791.

22. Flotte, T.R. (2020). Revisiting the "New" Inflammatory Toxicities of Adeno-Associated Virus Vectors. Hum. Gene Ther. 31, 398–399.

23. Shen, W., Liu, S., and Ou, L. (2022). rAAV immunogenicity, toxicity, and durability in 255 clinical trials: A meta-analysis. Front. Immunol. 13, 1104646.

24. Ertl, H.C.J. (2022). Immunogenicity and toxicity of AAV gene therapy. Front. Immunol. 13, 975803.

25. Mueller, C., Berry, J.D., McKenna-Yasek, D.M., Gernoux, G., Owegi, M.A., Pothier, L.M., Douthwright, C.L., Gelevski, D., Luppino, S.D., Blackwood, M., et al. (2020). SOD1 Suppression with Adeno-Associated Virus and MicroRNA in Familial ALS. N. Engl. J. Med. 383, 151–158.

26. Duan, D. (2023). Lethal immunotoxicity in high-dose systemic AAV therapy. Mol. Ther. 31, 3123–3126.

27. Sabatino, D.E., and McCarty, D.M. (2021). Topics in AAV integration come front and center at ASGCT AAV Integration Roundtable. Mol. Ther. 29, 3319–3320.

28. Manno, C.S., Chew, A.J., Hutchison, S., Larson, P.J., Herzog, R.W., Arruda, V.R., Tai, S.J., Ragni, M.V., Thompson, A., Ozelo, M., et al. (2003). AAV-mediated factor IX gene transfer to skeletal muscle in patients with severe hemophilia B. Blood 101, 2963–2972.

29. Greig, J.A., Calcedo, R., Grant, R.L., Peng, H., Medina-Jaszek, C.A., Ahonkhai, O., Qin, Q., Roy, S., Tretiakova, A.P., and Wilson, J.M. (2016). Intramuscular administration of AAV overcomes pre-existing neutralizing antibodies in rhesus macaques. Vaccine 34, 6323–6329.

30. Flotte, T.R., Trapnell, B.C., Humphries, M., Carey, B., Calcedo, R., Rouhani, F., Campbell-Thompson, M., Yachnis, A.T., Sandhaus, R.A., McElvaney, N.G., et al. (2011). Phase 2 clinical trial of a recombinant adeno-associated viral vector expressing α1-antitrypsin: interim results. Hum. Gene Ther. 22, 1239–1247.

31. Brantly, M.L., Chulay, J.D., Wang, L., Mueller, C., Humphries, M., Spencer, L.T., Rouhani, F., Conlon, T.J., Calcedo, R., Betts, M.R., et al. (2009). Sustained transgene expression despite T lymphocyte responses in a clinical trial of rAAV1-AAT gene therapy. Proc. Natl. Acad. Sci. USA 106, 16363–16368.

32. Costa-Verdera, H., Unzu, C., Valeri, E., Adriouch, S., González Aseguinolaza, G., Mingozzi, F., and Kajaste-Rudnitski, A. (2023). Understanding and Tackling Immune Responses to Adeno-Associated Viral Vectors. Hum. Gene Ther. 34, 836–852.

33. Nakamura, A., and Terauchi, Y. (2013). Lessons from mouse models of high-fat diet-induced NAFLD. Int. J. Mol. Sci. 14, 21240–21257.

34. Tsuchida, T., and Friedman, S.L. (2017). Mechanisms of hepatic stellate cell activation. Nat. Rev. Gastroenterol. Hepatol. 14, 397–411.

35. Higashi, T., Friedman, S.L., and Hoshida, Y. (2017). Hepatic stellate cells as key target in liver fibrosis. Adv. Drug Deliv. Rev. 121, 27–42.

36. Ogawa, Y., Kurosu, H., Yamamoto, M., Nandi, A., Rosenblatt, K.P., Goetz, R., Eliseenkova, A.V., Mohammadi, M., and Kuro-O, M. (2007). BetaKlotho is required for metabolic activity of fibroblast growth factor 21. Proc. Natl. Acad. Sci. USA 104, 7432–7437.

37. Hill-Baskin, A.E., Markiewski, M.M., Buchner, D.A., Shao, H., DeSantis, D., Hsiao, G., Subramaniam, S., Berger, N.A., Croniger, C., Lambris, J.D., and Nadeau, J.H. (2009). Diet-induced hepatocellular carcinoma in genetically predisposed mice. Hum. Mol. Genet. 18, 2975–2988.

38. Ribas, V., de la Rosa, L.C., Robles, D., Núñez, S., Segalés, P., Insausti-urkia, N., Solsona-vilarrasa, E., Fernández-Checa, J.C., and García-Ruiz, C. (2021). Dietary and Genetic Cholesterol Loading Rather Than Steatosis Promotes Liver Tumorigenesis and NASH-Driven HCC. Cancers (Basel) 13, 4091.

39. Considine, R.V., Sinha, M.K., Heiman, M.L., Kriauciunas, A., Stephens, T.W., Nyce, M.R., Ohannesian, J.P., Marco, C.C., McKee, L.J., Bauer, T.L., et al. (1996). Serum immunoreactive-leptin concentrations in normal-weight and obese humans. N. Engl. J. Med. 334, 292–295.

40. Boutari, C., and Mantzoros, C.S. (2020). Adiponectin and leptin in the diagnosis and therapy of NAFLD. Metabolism 103, 154028.

41. Guillemot-Legris, O., and Muccioli, G.G. (2017). Obesity-Induced Neuroinflammation: Beyond the Hypothalamus. Trends Neurosci. 40, 237–253.

42. Amiri, S., and Behnezhad, S. (2019). Obesity and anxiety symptoms: a systematic review and meta-analysis. Neuropsychiatr. 33, 72–89.

43. Seebacher, F., Tallis, J., McShea, K., and James, R.S. (2017). Obesity-induced decreases in muscle performance are not reversed by weight loss. Int. J. Obes. 41, 1271–1278.

44. Pérez, L.M., Pareja-Galeano, H., Sanchis-Gomar, F., Emanuele, E., Lucia, A., and Gálvez, B.G. (2016). "Adipaging": ageing and obesity share biological hallmarks related to a dysfunctional adipose tissue. J. Physiol. 594, 3187–3207.

45. Medina-Julio, D., Ramírez-Mejía, M.M., Cordova-Gallardo, J., Peniche-Luna, E., Cantú-Brito, C., and Mendez-Sanchez, N. (2024). From Liver to Brain: How MAFLD/MASLD Impacts Cognitive Function. Med. Sci. Monit. 30, e943417.

46. Hsuchou, H., Pan, W., and Kastin, A.J. (2007). The fasting polypeptide FGF21 can enter brain from blood. Peptides (N.Y.) 28, 2382–2386.

47. Hamed, S.A. (2017). Brain injury with diabetes mellitus: evidence, mechanisms and treatment implications. Expert Rev. Clin. Pharmacol. 10, 409–428.

48. Flores-Cordero, J.A., Pérez-Pérez, A., Jiménez-Cortegana, C., Alba, G., Flores-Barragán, A., and Sánchez-Margalet, V. (2022). Obesity as a Risk Factor for Dementia and Alzheimer's Disease: The Role of Leptin. Int. J. Mol. Sci. 23, 5202.

49. Misiak, B., Leszek, J., and Kiejna, A. (2012). Metabolic syndrome, mild cognitive impairment and Alzheimer's disease–the emerging role of systemic low-grade inflammation and adiposity. Brain Res. Bull. 89, 144–149.

50. Giralt, M., Gavaldà-Navarro, A., and Villarroya, F. (2015). Fibroblast growth factor-21, energy balance and obesity. Mol. Cell. Endocrinol. 418, 66–73.

51. Singhal, G., Kumar, G., Chan, S., Fisher, F.M., Ma, Y., Vardeh, H.G., Nasser, I.A., Flier, J.S., and Maratos-Flier, E. (2018). Deficiency of fibroblast growth factor 21 (FGF21) promotes hepatocellular carcinoma (HCC) in mice on a long term obesogenic diet. Mol. Metab. 13, 56–66.

52. Liu, X., Zhang, P., Martin, R.C., Cui, G., Wang, G., Tan, Y., Cai, L., Lv, G., and Li, Y. (2016). Lack of fibroblast growth factor 21 accelerates metabolic liver injury characterized by steatohepatitis in mice. Am. J. Cancer Res. 6, 1011–1025.

53. Zhang, Q., Li, Y., Liang, T., Lu, X., Liu, X., Zhang, C., Jiang, X., Martin, R.C., Cheng, M., and Cai, L. (2015). Loss of FGF21 in diabetic mouse during hepatocellular carcinogenetic transformation. Am. J. Cancer Res. 5, 1762–1774.

54. Huang, X., Yu, C., Jin, C., Yang, C., Xie, R., Cao, D., Wang, F., and McKeehan, W.L. (2006). Forced expression of hepatocyte-specific fibroblast growth factor 21 delays initiation of chemically induced hepatocarcinogenesis. Mol. Carcinog. 45, 934–942.

55. Xu, P., Zhang, Y., Wang, W., Yuan, Q., Liu, Z., Rasoul, L.M., Wu, Q., Liu, M., Ye, X., Li, D., and Ren, G. (2015). Long-Term Administration of Fibroblast Growth Factor 21 Prevents Chemically-Induced Hepatocarcinogenesis in Mice. Dig. Dis. Sci. 60, 3032–3043.

56. Verzijl, C.R.C., Van De Peppel, I.P., Struik, D., and Jonker, J.W. (2020). Pegbelfermin (BMS-986036): an investigational PEGylated fibroblast growth factor 21 analogue for the treatment of nonalcoholic steatohepatitis. Expert Opin. Investig. Drugs 29, 125–133.

57. Bailey, N.N., Peterson, S.J., Parikh, M.A., Jackson, K.A., and Frishman, W.H. (2023). Pegozafermin Is a Potential Master Therapeutic Regulator in Metabolic Disorders: A Review. Cardiol. Rev. https://doi.org/10.1097/CRD.0000000000000625.

58. Puengel, T., and Tacke, F. (2023). Efruxifermin, an investigational treatment for fibrotic or cirrhotic nonalcoholic steatohepatitis (NASH). Expert Opin. Investig. Drugs 32, 451–461.

59. Wharton, S., Haase, C.L., Kamran, E., Liu, A., Mancini, J., Neish, D., Pakseresht, A., Power, G.S., and Christensen, R.A.G. (2020). Weight loss and persistence with liraglutide 3.0 mg by obesity class in the real-world effectiveness study in Canada. Obes. Sci. Pract. 6, 439–444.

60. Ganguly, R., Tian, Y., Kong, S.X., Hersloev, M., Hobbs, T., Smolarz, B.G., Ramasamy, A., Haase, C.L., and Weng, W. (2018). Persistence of newer anti-obesity medications in a real-world setting. Diabetes Res. Clin. Pract. 143, 348–356.

61. Weiss, T., Yang, L., Carr, R.D., Pal, S., Sawhney, B., Boggs, R., Rajpathak, S., and Iglay, K. (2022). Real-world weight change, adherence, and discontinuation among patients with type 2 diabetes initiating glucagon-like peptide-1 receptor agonists in the UK. BMJ Open Diabetes Res. Care 10, e002517.

62. Weiss, T., Carr, R.D., Pal, S., Yang, L., Sawhney, B., Boggs, R., Rajpathak, S., and Iglay, K. (2020). Real-World Adherence and Discontinuation of Glucagon-Like Peptide-1

63. Receptor Agonists Therapy in Type 2 Diabetes Mellitus Patients in the United States. Patient Prefer. Adherence 14, 2337–2345.

63. Adams, A.C., Halstead, C.A., Hansen, B.C., Irizarry, A.R., Martin, J.A., Myers, S.R., Reynolds, V.L., Smith, H.W., Wroblewski, V.J., and Kharitonenkov, A. (2013). LY2405319, an Engineered FGF21 Variant, Improves the Metabolic Status of Diabetic Monkeys. PLoS One 8, e65763.

64. Stanislaus, S., Hecht, R., Yie, J., Hager, T., Hall, M., Spahr, C., Wang, W., Weiszmann, J., Li, Y., Deng, L., et al. (2017). A novel Fc-FGF21 with improved resistance to proteolysis, increased affinity toward β-klotho, and enhanced efficacy in mice and cynomolgus monkeys. Endocrinology 158, 1314–1327.

65. Gaich, G., Chien, J.Y., Fu, H., Glass, L.C., Deeg, M.A., Holland, W.L., Kharitonenkov, A., Bumol, T., Schilske, H.K., and Moller, D.E. (2013). The effects of LY2405319, an FGF21 Analog, in obese human subjects with type 2 diabetes. Cell Metab. 18, 333–340.

66. Talukdar, S., Zhou, Y., Li, D., Rossulek, M., Dong, J., Somayaji, V., Weng, Y., Clark, R., Lanba, A., Owen, B.M., et al. (2016). A long-acting FGF21 molecule, PF-05231023, decreases body weight and improves lipid profile in non-human primates and type 2 diabetic subjects. Cell Metab. 23, 427–440.

67. Kim, A.M., Somayaji, V.R., Dong, J.Q., Rolph, T.P., Weng, Y., Chabot, J.R., Gropp, K.E., Talukdar, S., and Calle, R.A. (2017). Once-weekly administration of a long-acting fibroblast growth factor 21 analogue modulates lipids, bone turnover markers, blood pressure and body weight differently in obese people with hypertriglyceridaemia and in non-human primates. Diabetes Obes. Metab. 19, 1762–1772.

68. Abdelmalek, M.F., Sanyal, A.J., Nakajima, A., Neuschwander-Tetri, B.A., Goodman, Z.D., Lawitz, E.J., Harrison, S.A., Jacobson, I.M., Imajo, K., Gunn, N., et al. (2024). Pegbelfermin in Patients With Nonalcoholic Steatohepatitis and Compensated Cirrhosis (FALCON 2): A Randomized Phase 2b Study. Clin. Gastroenterol. Hepatol. 22, 113–123.e9.

69. Loomba, R., Lawitz, E.J., Frias, J.P., Ortiz-Lasanta, G., Johansson, L., Franey, B.B., Morrow, L., Rosenstock, M., Hartsfield, C.L., Chen, C.-Y., et al. (2023). Safety, pharmacokinetics, and pharmacodynamics of pegozafermin in patients with non-alcoholic steatohepatitis: a randomised, double-blind, placebo-controlled, phase 1b/2a multiple-ascending-dose study. Lancet Gastroenterol. Hepatol. 8, 120–132.

70. Rosenstock, M., Tseng, L., Pierce, A., Offman, E., Chen, C.Y., Charlton, R.W., Margalit, M., and Mansbach, H. (2023). The Novel GlycoPEGylated FGF21 Analog Pegozafermin Activates Human FGF Receptors and Improves Metabolic and Liver Outcomes in Diabetic Monkeys and Healthy Human Volunteers. J. Pharmacol. Exp. Ther. 387, 204–213.

71. Harrison, S.A., Ruane, P.J., Freilich, B., Neff, G., Patil, R., Behling, C., Hu, C., Shringarpure, R., de Temple, B., Fong, E., et al. (2023). A randomized, double-blind, placebo-controlled phase IIa trial of efruxifermin for patients with compensated NASH cirrhosis. JHEP Rep. 5, 100563.

72. Harrison, S.A., Ruane, P.J., Freilich, B.L., Neff, G., Patil, R., Behling, C.A., Hu, C., Fong, E., de Temple, B., Tillman, E.J., et al. (2021). Efruxifermin in non-alcoholic steatohepatitis: a randomized, double-blind, placebo-controlled, phase 2a trial. Nat. Med. 27, 1262–1271.

73. Harrison, S.A., Frias, J.P., Neff, G., Abrams, G.A., Lucas, K.J., Sanchez, W., Gogia, S., Sheikh, M.Y., Behling, C., Bedossa, P., et al. (2023). Safety and efficacy of once-weekly efruxifermin versus placebo in non-alcoholic steatohepatitis (HARMONY): a multicentre, randomised, double-blind, placebo-controlled, phase 2b trial. Lancet Gastroenterol. Hepatol. 8, 1080–1093.

74. George, L.A., Sullivan, S.K., Giermasz, A., Rasko, J.E.J., Samelson-Jones, B.J., Ducore, J., Cuker, A., Sullivan, L.M., Majumdar, S., Teitel, J., et al. (2017). Hemophilia B Gene Therapy with a High-Specific-Activity Factor IX Variant. N. Engl. J. Med. 377, 2215–2227.

75. Falk, D.J., Soustek, M.S., Todd, A.G., Mah, C.S., Cloutier, D.A., Kelley, J.S., Clement, N., Fuller, D.D., and Byrne, B.J. (2015). Comparative impact of AAV and enzyme replacement therapy on respiratory and cardiac function in adult Pompe mice. Mol. Ther. Methods Clin. Dev. 2, 15007.

76. Costa-Verdera, H., Collaud, F., Riling, C.R., Sellier, P., Nordin, J.M.L., Preston, G.M., Cagin, U., Fabregue, J., Barral, S., Moya-Nilges, M., et al. (2021). Hepatic expression of GAA results in enhanced enzyme bioavailability in mice and non-human primates. Nat. Commun. 12, 6393.

77. Loomba, R., Sanyal, A.J., Kowdley, K.V., Bhatt, D.L., Alkhouri, N., Frias, J.P., Bedossa, P., Harrison, S.A., Lazas, D., Barish, R., et al. (2023). Randomized, Controlled Trial of the FGF21 Analogue Pegozafermin in NASH. N. Engl. J. Med. 389, 998–1008.

78. Sanyal, A., Charles, E.D., Neuschwander-Tetri, B.A., Loomba, R., Harrison, S.A., Abdelmalek, M.F., Lawitz, E.J., Halegoua-DeMarzio, D., Kundu, S., Noviello, S., et al. (2019). Pegbelfermin (BMS-986036), a PEGylated fibroblast growth factor 21 analogue, in patients with non-alcoholic steatohepatitis: a randomised, double-blind, placebo-controlled, phase 2a trial. The Lancet 392, 2705–2717.

79. Ayuso, E., Mingozzi, F., Montane, J., Leon, X., Anguela, X.M., Haurigot, V., Edmonson, S.A., Africa, L., Zhou, S., High, K.A., et al. (2010). High AAV vector purity results in serotype- and tissue-independent enhancement of transduction efficiency. Gene Ther. 17, 503–510.

80. Haurigot, V., Marcó, S., Ribera, A., Garcia, M., Ruzo, A., Villacampa, P., Ayuso, E., Añor, S., Andaluz, A., Pineda, M., et al. (2013). Whole body correction of mucopolysaccharidosis IIIA by intracerebrospinal fluid gene therapy. J. Clin. Invest. 123, 3254–3271.

81. Leger, M., Quiedeville, A., Bouet, V., Haelewyn, B., Boulouard, M., Schumann-Bard, P., and Freret, T. (2013). Object recognition test in mice. Nat. Protoc. 8, 2531–2537.

82. Carr, T.P., Andresen, C.J., and Rudel, L.L. (1993). Enzymatic determination of triglyceride, free cholesterol, and total cholesterol in tissue lipid extracts. Clin. Biochem. 26, 39–42.

83. Muñoz-Prieto, A., Cerón, J.J., Martínez-Subiela, S., Mrljak, V., and Tvarijonaviciute, A. (2020). A Systematic Review and Meta-Analysis of Serum Adiponectin Measurements in the Framework of Dog Obesity. Animals (Basel) 10, 1–15.

84. Tvarijonaviciute, A., Martínez-Subiela, S., and Ceron, J.J. (2010). Validation of 2 commercially available enzyme-linked immunosorbent assays for adiponectin determination in canine serum samples. Can J. Vet. Res. 74, 279–285.

85. Nakade, Y., Sakamoto, K., Yamauchi, T., Inoue, T., Kobayashi, Y., Yamamoto, T., Ishii, N., Ohashi, T., Sumida, Y., Ito, K., et al. (2017). Conophylline inhibits non-alcoholic steatohepatitis in mice. PLoS One 12, e0178436.

86. Munoz, S., Franckhauser, S., Elias, I., Ferre, T., Hidalgo, A., Monteys, A.M., Molas, M., Cerdan, S., Pujol, A., Ruberte, J., et al. (2010). Chronically increased glucose uptake by adipose tissue leads to lactate production and improved insulin sensitivity rather than obesity in the mouse. Diabetologia 53, 2417–2430.

87. Jimenez, V., Ayuso, E., Mallol, C., Agudo, J., Casellas, A., Obach, M., Muñoz, S., Salavert, A., and Bosch, F. (2011). In vivo genetic engineering of murine pancreatic beta cells mediated by single-stranded adeno-associated viral vectors of serotypes 6, 8 and 9. Diabetologia 54, 1075–1086.